Photons to Formate: A Review on Photocatalytic Reduction of CO_2 to Formic Acid

Hanqing Pan and Michael D. Heagy *,†

Department of Chemistry, New Mexico Institute of Mining and Technology, Socorro, NM 87801, USA; hanqing.pan@student.nmt.edu

* Correspondence: mdhsch@rit.edu

† Current Address: School of Chemistry and Materials Science, Rochester Institute of Technology, 84 Lomb Memorial Drive, Rochester, New York, NY 14623, USA.

check for updates

Abstract: Rising levels of atmospheric carbon dioxide due to the burning and depletion of fossil fuels is continuously raising environmental concerns about global warming and the future of our energy supply. Renewable energy, especially better utilization of solar energy, is a promising method for CO_2 conversion and chemical storage. Research in the solar fuels area is focused on designing novel catalysts and developing new conversion pathways. In this review, we focus on the photocatalytic reduction of CO_2 primarily in its neutral pH species of carbonate to formate. The first two-electron photoproduct of carbon dioxide, a case for formate (or formic acid) is made in this review based on its value as; an important chemical feedstock, a hydrogen storage material, an intermediate to methanol, a high-octane fuel and broad application in fuel cells. This review focuses specifically on the following photocatalysts: semiconductors, phthalocyanines as photosensitizers and membrane devices and metal-organic frameworks.

Keywords: CO_2 reduction; formate; photocatalyst

1. Introduction

The sun provides 100,000 TW of energy in one hour that is enough to power the earth for one year, [1] but the energy needs to be storable and transportable (i.e., chemical fuel) because renewable energy sources generally provide an intermittent supply of energy [2]. In principle, all terrestrial energy sources, such as fossil fuels and uranium, can be considered as a solar fuel; it just depends on the time frame. For the purpose of this review, when solar energy is converted into chemical fuel on a diurnal basis the term solar fuels applies. As a mitigation strategy, C1 sources such as CO_2 or its pH neutral dissolved version, bicarbonate become concentrated energy sources for long-term storage capacity via energy input from solar irradiation [3]. In 2019, fossil fuels still supply 84% of the world's energy [4]. In addition to limitations in the availability of fossil fuels, the emission of greenhouse gases, especially carbon dioxide, upon the combustion of fossil fuels is a major contributor to rising levels of anthropogenic carbon dioxide in the atmosphere. With the limitations in availability of fossil fuels, new sources of energy that provide a large-scale, sustainable energy supply must be developed. Solar energy is the most abundant renewable energy source available that can meet our future energy demands [5]. One potential approach towards generating renewable fuels is to use solar energy to directly reduce atmospheric or locally produced CO_2 to liquid fuels. This approach, referred to as "chemical carbon mitigation" can lead to methanol as an end product, a useful solar fuel. The concept of "the methanol economy," championed by Chemistry Nobel laureate George Olah, highlights methanol as a renewable and readily transportable fuel and an alternative to the hydrogen economy. A key component to several C1 conversion methods in the methanol economy is

the solar-driven conversion of carbon dioxide to formic acid and ultimately to methanol, a renewable and regenerative C1 fuel [6–8].

The photocatalytic reduction of CO_2 is a multi-electron transfer process that can lead to the formation of many different products depending on the reaction pathway and the number of electrons transferred. Two-electron products include carbon monoxide, formic acid and oxalate. Methanol is the six-electron product and methane is the result of eight electron transfers [9–13]. The reduction half-reaction utilizes the photogenerated electrons, leaving behind the photogenerated holes. Ideally, the oxidation half-reaction would lead to the oxidation of water generating hydrogen or oxygen but very few systems can accomplish simultaneous oxidation and reduction reactions [9]. Therefore, research has focused on developing a sacrificial agent that can efficiently scavenge the photogenerated holes.

Photocatalysis follows three key steps (Figure 1): (1) Photon absorption by semiconductor, (2) charge separation, (3) surface reactions. Semiconductors are attractive materials for photocatalysis because their band gap energies are similar to that of UV or visible light (Figure 2) [9]. Upon absorption of a photon with energy greater or equal to the band gap of the semiconductor, an electron is excited from the valence band to the conduction band, leaving behind a hole. The photo-generated charge carriers then migrate to the semiconductor surface and transfer to the adsorbed molecules, which initiates the subsequent oxidation or reduction reactions. The formation of charge carriers is followed by several de-excitation pathways (Figure 1). Transfer of the charge carrier, either electron or hole, to the acceptor molecules leads to its oxidation or reduction (pathway 3 and 4). The carriers can recombine with the opposite charge carrier trapped at the surface (pathway 5) or recombination can occur in the bulk of the semiconductor (pathway 6). Three major drawbacks of photocatalysis include (1) narrow region of optical absorption, (2) rapid electron/hole recombination and (3) lack of understanding of photocatalysis mechanisms. This review aims to address these challenges.
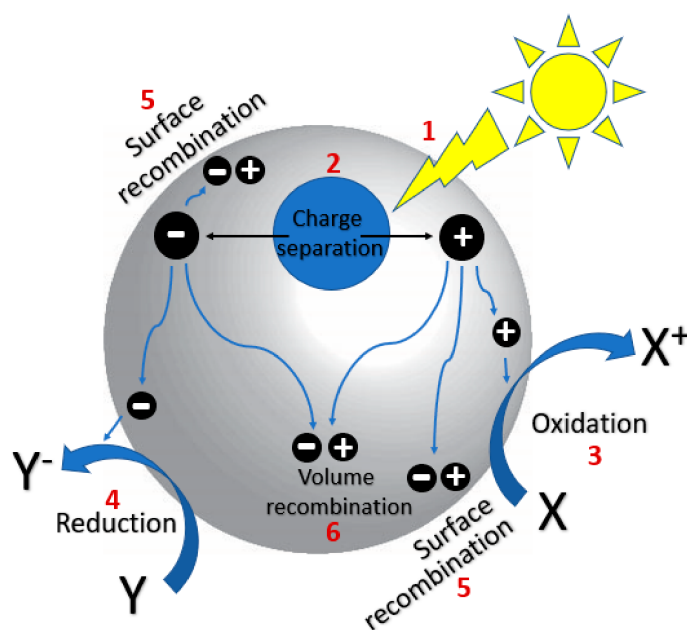

Figure 1. Photo-excitation of a semiconductor and subsequent generation of charge carriers and decay pathways. X = electron donor, Y = electron acceptor.
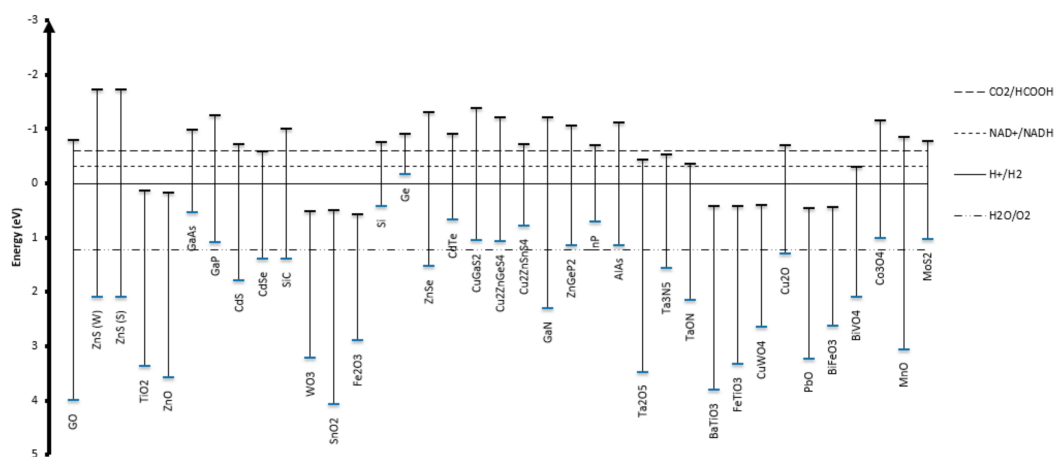
Figure 2. Valence and conduction band edge potentials of various semiconductors, along with reduction potentials for $CO_2/HCOOH$, $NAD^+/NADH$, H^+/H_2 and H_2O/O_2.

This review is structured as follows: Sections 2 and 3 discusses the fundamentals of photocatalytic CO_2 reduction and explains why our work is focused on photocatalytic bicarbonate reduction to formate. Section 4 divides the catalysts into semiconductors, phthalocyanine-semiconductors and metal-organic frameworks. Lastly, Section 5 discusses the outlook of photochemical CO_2 reduction to formate and Section 6 summarizes the review with concluding remarks.

2. Fundamentals of Photocatalytic CO_2 Reduction

Thermodynamics of CO_2 Reduction

Photocatalytic reduction of CO_2 has a positive $\Delta G°$ value, meaning the process is non-spontaneous and requires significant energy input from the incident photons. As mentioned previously, methanol production from CO_2 reduction requires six protons and six electrons. Recently, there are studies in which homogeneous sensitizers coupled with metal co-catalysts have been shown to produce only CO and formic acid [14]. This observation of the incomplete six-electron reduction to methanol is governed by thermodynamics. Methanol production in an aqueous medium at pH 7 occurs at a slightly more positive potential (-0.39 V vs. NHE) than formate (-0.58 V vs. NHE) (Table 1). In addition, reduction of CO_2 to formate only requires two electrons whereas reduction to methanol requires six.

Table 1. The main products of CO_2 and water reduction and the corresponding reduction potentials with reference to NHE at pH 7 in aqueous solution [13,15].

Product	Reaction	E° (V vs. NHE)	Equation
Hydrogen	$2H_2O + 2e^- \rightarrow 2OH^- + H_2$	-0.41	(1)
Methane	$CO_2 + 8H^+ + 8e^- \rightarrow CH_4 + 2H_2O$	-0.24	(2)
Carbon monoxide	$CO_2 + 2H^+ + 2e^- \rightarrow CO + H_2O$	-0.51	(3)
Methanol	$CO_2 + 6H^+ + 6e^- \rightarrow CH_3OH + H_2O$	-0.39	(4)
Formic acid	$CO_2 + 2H^+ + 2e^- \rightarrow HCOOH$	-0.58	(5)
Ethane	$2CO_2 + 14H^+ + 14e^- \rightarrow C_2H_6 + 4H_2O$	-0.27	(6)
Ethanol	$2CO_2 + 12H^+ + 12e^- \rightarrow C_2H_5OH + 3H_2O$	-0.33	(7)
Oxalate	$2CO_2 + 2H^+ + 2e^- \rightarrow H_2C_2O_4$	-0.87	(8)

Since carbon is in its highest oxidized state in CO_2, its reduction can lead to a wide variety of products (CO, CH_4, CH_3OH, HCOOH and many other products). CO_2 is a thermodynamically stable and chemically inert molecule with the C=O bond possessing a high dissociation energy of ~750 kJ/mol and C-C bond of ~336 kJ/mol, indicating a significant amount of energy input [16,17]. Moreover, the breaking of the C=O bonds and the bending of the molecular from linear to bent has

been shown to require a large input of energy [18]. In addition, Equation (9) has been shown to be the necessary step to activate CO_2, which has a very negative potential; therefore, high overpotential is needed to convert a CO_2 molecule to products [9,13].

$$CO_2 + e^- \rightarrow CO_2^{\bullet -} \qquad E° = -1.90 \text{ V vs. NHE} \tag{9}$$

We chose to highlight bicarbonate reduction in this study because of its reduction efficiency over dissolved CO_2 gas due to its limited solubility of CO_2 in water (0.033 M at 298 K and 1 atm) [19]. As several reports require the use of aqueous conditions, bubbled CO_2 poses a concentration disadvantage. In a previous study by our group [20], we questioned the standard assumption that CO_2 was the only species undergoing reduction even though numerous publications were using a bicarbonate buffer. This paper was among the first to conduct a control experiment with only bicarbonate buffer and no bubbled CO_2 [21,22]. From this control experiment, we discovered that bubbling CO_2 did not result in significantly higher formate production. Consequently, we decided to focus our efforts on bicarbonate reduction due to the following major issues with CO_2. First, a considerable practical problem with atmospheric capture is that the concentration of CO_2 in the air is still fairly low at 100's of ppm [23]. While several concentrated CO_2 sources exist at fossil fuel burning plants or in some cases oil drilling activities, it is very hard to supply a reactor with enough CO_2 if it is being drawn from the atmosphere. Our experimental conditions parallel ocean bicarbonate concentration of 0.033 M [19] and with the continual acidification of the ocean due to dissolved carbon dioxide, it is relevant to capture bicarbonate and convert it to a value-added product.

3. The Case for Photons to Formate

In comparison to hydrogen, fuels based on carbon hold the advantage when it comes to denser volumetric energy along with transportation and storage within the current industrialized infrastructure. Converting CO_2 into value-added chemicals could contribute to negative emission technologies (NETs) by carbon sequestration into acetic acid, ethylene and formic acid instead of expensive geological storage [11]. Of these commodity chemicals, formate production and its growing chemical application has increased significantly over the past decade [24]. Furthermore, in relation to higher C_n homologs, CO_2 reduction to specialty chemicals in the range of C_1-C_3 such as formic acid production (0.2 MtC/yr) or propanol (0.1 MtC/yr) offers a brighter outlook for near term economic sustainability [25–27]. By comparison, carbon mitigation at the GtC/yr scale, which is ultimately impactful toward global climate change, will necessitate chemical conversion of greenhouse gases to be competitive with the production of fossil fuels such as coal (4 GtC/yr) and natural gas (1.4 GtC/yr) [28,29].

Techno-Economic Analysis

Even though CO_2 reduction is a widely studied field, much of the research is focused on the fundamental aspects of catalyst design and product selectivity. However, for this process to be commercialized, many requirements need to be met such as (1) continuous operation, (2) high product selectivity and throughput and (3) long-term stable operation [30]. In addition, it is essential that the energy used in the CO_2 conversion process does not generate additional CO_2. Recent studies on the economic feasibility of a commercial CO_2 reduction reactor show that formic acid is one of the only products that has potential to be made on a large-scale basis. Jouny et al. calculated the end-of-life net present value (NPV) of a CO_2 electrolyzer for the production of 100 tons/day of various CO_2 reduction products and found that only carbon monoxide and formic acid were the only economically viable products with NPVs of $13.5 million and $39.4 million, respectively [25]. Spurgeon and Kumar analyzed electrochemical conversion of flue gas CO_2 to liquid products and found that electrosynthesized formic acid from CO_2 was analyzed to be near market prices as a bulk chemical, even though it is not promising as an economic fuel. The major issue was the high capital cost for CO_2 electrolyzers since high Faradaic efficiency, high current densities and reduced electrolyzer

cost is necessary for economic viability [31]. Rumayor et al. carried out a techno-economic analysis of electrochemical reduction of CO_2 to formic acid and found that it is not yet profitable and competitive under current market conditions due to the high production costs [32].

4. Photocatalytic CO_2 Reduction to Formic Acid

4.1. Semiconductors

Halmann and Inoue were the first to reduce CO_2 with semiconductor photocatalysts. Within a year of each other, both published their works in *Nature* reported the photo-reduction of CO_2 in aqueous medium. In 1978, Halmann constructed a photoelectrode consisting of p-type gallium phosphide that produced formic acid after 18 h of irradiation [33]. A year later, Inoue reported the reduction of CO_2 using several photosensitive semiconductor powders (TiO_2, ZnO, CdS, GaP, SiC and WO_3) suspended in water [34]. Inoue's work was one of the first studies to hypothesize that for photocatalysis to be efficient, photo-excited electrons in the more negative conduction band have greater ability to reduce carbon dioxide. Even though this work produced low quantum yields (0.0005%), it was an important early study that inspired many other researchers. Following these two papers, both authors continued to make novel discoveries in this field. Halmann, in 1982, demonstrated enhanced formate production could be achieved by using oxides of rare earth dopants (Eu_2O_3, Sm_2O_3, Nd_2O_3, CeO_2) to dope large band gap semiconductors ($BaTiO_3$, $LiNbO_3$) [35]. The optical properties of the catalysts were studied by diffuse reflectance spectroscopy, which uncovered the fact that rare earth dopants allowed the extension of optical absorption in the visible region of approximately 600 nm. A year later, Halmann reported the photoelectrochemical reduction of aqueous CO_2 using a single crystal p-gallium phosphide and p-gallium arsenide as photocathodes in neutral or weakly acidic medium [36]. The main product was determined to be formate (71 µmol) but formaldehyde and methanol were also produced. The influence of pH on the behavior of the electrodes was studied and a strong photo-effect was seen for all pH values. The next year, Halmann once again studied TiO_2 in the photo-reduction of CO_2, this time doped with RuO_2 [37]. They found that by doping anatase TiO_2 with RuO_2, formate was the predominant product and efficiency reached 0.04%. Later in 1995, Inoue reported on the photoreduction of CO_2 using chalcogenide semiconductor microcrystals. This study synthesized cadmium-loaded ZnS microcrystals in a sodium bicarbonate buffer and bubbled CO_2, which produced the highest quantum efficiency of 32.5%, twice as large as that obtained on bare ZnS microcrystals. However, the quantum efficiency was determined using 280 nm irradiation, which would explain the high efficiency by using monochromatic light. 2-propanol was used as a hole scavenger and it was found that Cd loading was an important factor in formate production. It was also reported that with increasing mole fraction of Cd, formate production actually decreased and that the optimal Cd loading is 0.5–0.67%. Other metals such as Pb, Ni, Ag and Cu were used but none produced as high efficiency as Cd-ZnS [38].

Since the work by Inoue, ZnS has become an attractive semiconductor photocatalyst because of its non-toxic and earth abundant attributes and its effectiveness in the reduction of CO_2. Kanemoto was able to achieve sufficient formate production of 75.1 µmol/h but this experiment was performed at 313 nm irradiation [39]. These findings also confirmed 2-propanol to be the most efficient electron donor amid sodium phosphate, sodium sulfate and triethanolamine. Johne and Kisch loaded ZnS onto large surface area SiO_2 particles to produce formate under UV irradiation. Later, 2,5-dihydrofuran was used as a reducing agent, which assisted in the production of 7000 µmol of formate [40].

Our group recently explored the photoreduction of bicarbonate to formate using wurtzite and sphalerite ZnS particles [20]. ZnS was studied in depth under the parameters of size, crystal lattice, surface area and band gap on the productivity of formate. Photochemical experiments were performed under air mass coefficient (AM 1.5 and 0) solar simulator conditions. Formate production was negligible under AM 1.5 conditions but significantly increased under AM 0 conditions due to the inclusion of shorter wavelength photons. This work was one of the first to question the standard assumption that CO_2 is the only species undergoing reduction. Compared to earlier works reporting bubbled CO_2 in the

presence of bicarbonate, this work suggests that bicarbonate was the predominant species undergoing reduction. As the C-H bond undergoes oxidation in 2-propanol, glycerol with three hydroxylic positive hole scavengers was hypothesized as an improved semiconductor hole-scavenger and green chemistry solvent glycerol greatly improved the efficiency of the reaction. Continuing with ZnS, our group studied copper (I) oxide (Cu_2O) in the photoreduction of bicarbonate to formate. This work examined micron- and nano-particulate Cu_2O and synthesized a Ag/Cu_2O nanocomposite [41]. Due to plasmon-induced electron transfer from silver to Cu_2O, an enhanced formate production was found with the Ag/Cu_2O nanocomposite photocatalyst at 5.5% apparent quantum efficiency (Figure 3). In addition, an Au/TiO_2 and Ag/TiO_2 nanocomposite photocatalyst could reach apparent quantum efficiencies of 2.4% and 7.8%, respectively [42,43]. Beierle et al. designed a titanium nitride-titanium dioxide nanocomposite for bicarbonate reduction to formate. This work demonstrated that under solar illumination, the $TiN-TiO_2$ nanocomposite has higher photocatalytic activity than bare TiN or TiO_2, this nanocomposite can also greatly enhance formate production and remain stable for 8 h [44].
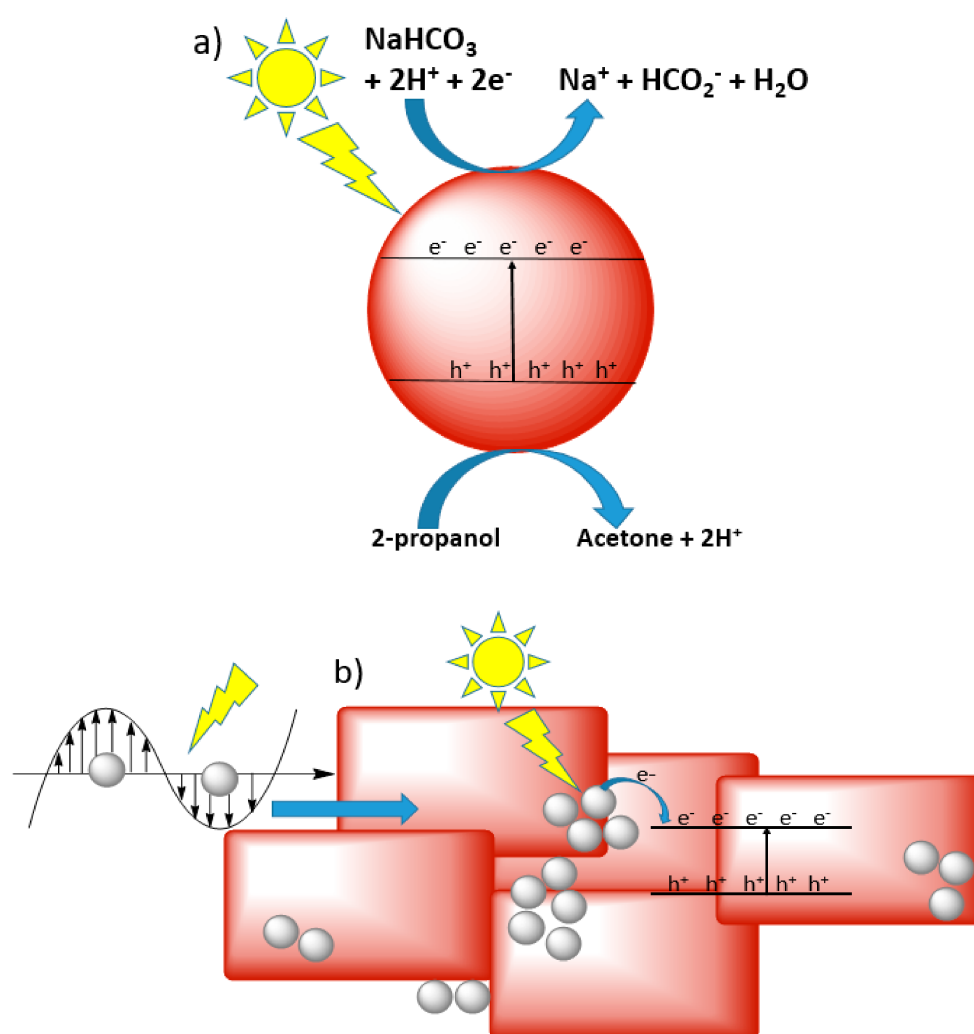

Figure 3. Proposed mechanism for (**a**) Cu_2O semiconductor and (**b**) Ag/Cu_2O (blue block arrow represents resonant energy transfer from metal to semiconductor). Reproduced from [41], with permission from American Chemical Society, 2018.

Baran et al. synthesized nanocrystalline zinc sulfide surface-modified with ruthenium(0) for the photocatalytic CO_2 reduction to formate, carbon monoxide and methane [45]. Formation of acetone was also observed due to the oxidation of the hole scavenger isopropanol. Surface-modified ZnS was more efficient than pure ZnS due to (1) the lowering of the CO_2 activation energy, (2) collection of electrons

at Ru particles resulted in a better charge separation and (3) better CO_2 desorption at the surface of modified ZnS. Both polar and non-polar solvents were tested and it was reported that in a polar solvent (water), formate is the major product and water was a better H-transfer agent than isopropanol. Kuwabata et al. employed ZnS microcrystallites for photocatalytic CO_2 reduction to methanol and formate by using methanol dehydrogenase and (MDH) and pyrroloquinoline quinone (PQQ) as an electron mediator for MDH and 2-propanol as a positive hole scavenger [46]. Acetone production resulting from the oxidation of 2-propanol was also studied.

Irvine et al. used CdS, ZnO, SiC, $BaTiO_3$ and $SrTiO_3$ to photochemically reduce aqueous CO_2 [47]. Product analysis showed the formation of formate, formaldehyde and methanol; the highest efficiency was obtained with ZnO, CdS and SiC. Continuing on Irvine's work, Eggins et al. used CdS or ZnS colloids for the photo-reduction of CO_2 to produce formate and other dimeric and tetrameric products such as oxalate, glyoxylate, glycolate and tartrate. Other semiconductors studied included ZnO, SiC, $BaTiO_3$ and $SrTiO_3$ [48]. This work discusses the role of several hole acceptor (or electron donor) compounds that assist in reacting with photogenerated holes. Different electron donors tested include iron ferracyanide, hydroquinone, 2-propanol, RuO_2 and hypophosphite. This paper highlights that semiconductors with the most negative conduction band potential results in the best quantum yields because they have a stronger reducing potential. This work concluded that ZnS resulted in the highest quantum yield among all the semiconductors tested. Henglein et al. reported the efficient photoreduction of CO_2 to formic acid using SiO_2-stabilized ZnS and 2-propanol as electron donor. By employing this system 0.80% AQE was achieved [49].

Kaneco and coworkers published three studies, all employing TiO_2 in a liquid CO_2 medium [50–52]. In the first effort, the effect of temperature, pressure, illumination time and surface area were examined. It was found that the formate yield was neither affected by temperature nor pressure. Formate production increased sharply with illumination time up until 5 h and progressed slowly until 30 h. A similar trend was observed with the surface area of the catalyst, formate increased linearly with increasing surface area of TiO_2 up to 0.4 m^2/g. Electron spin resonance elucidated the reaction mechanism of the reaction, which identified two radical species, photogenerated Ti^{3+} and $CO_2^{\bullet-}$ radical anion which resulted from the first electron transfer to CO_2. In their follow-up work, Kaneco and coworkers continued to investigate the photoreduction of high-pressure CO_2 using TiO_2 powders with 2-propanol as a positive hole scavenger [51]. Methane was found to be the main reduction product; formate was also detected but only under extremely high pressures of CO_2. In 1999, Kaneco and coworkers continued to study TiO_2 powders in supercritical fluid CO_2 by the investigation on the effects of temperature, pressure, irradiation time, surface area and aqueous solution for protonation. This study determined that formate production increased with an acidic pH medium because H^+ are advantageous for desorption of reaction intermediates from the surface of TiO_2 [52]. These two works were the first to point out that photo-excited TiO_2 results in $(Ti^{3+}\text{-}O^-)^*$ species (Figure 4) [51,52].

Liu et al. studied photocatalytic CO_2 reduction on CdS particles with and without surface modification in various solvents [53]. Formate and carbon monoxide were the two major products, as well as acetone from the oxidation of 2-propanol. The type of solvent and surface modification played a major role in the selectivity of the products. The reduction of CO_2 in acetonitrile produced carbon monoxide and formate, while in dichloromethane produced carbon monoxide only. Kisch reported CdS supported on silica and zinc sulfide to photocatalyze the reduction of bicarbonate to formate [54]. For CdS supported on zinc sulfide, it was found that the optimal CdS loading was 5%, which increased formate production 40-fold and 16-fold as compared to bare CdS and ZnS. Formate production was found to be dependent on bicarbonate concentration, when bicarbonate concentration increased from 33 to 60 mM formate production was enhanced by 10%. Formate production decreased by 20% when the pH was lowered to 5.3 but at a pH of 11.2, formate production increased by 25%. Zhang et al. used manganese sulfide (MnS) to reduce bicarbonate to formate at neutral pH [55]. Both ZnS and MnS have their conduction bands at highly reducing positions at −1.04 and −1.19 V versus NHE. This work

results in quantum efficiency of 4.2%, however, the wavelengths utilized fell within the UV region of the solar spectrum, between 200 and 400 nm.
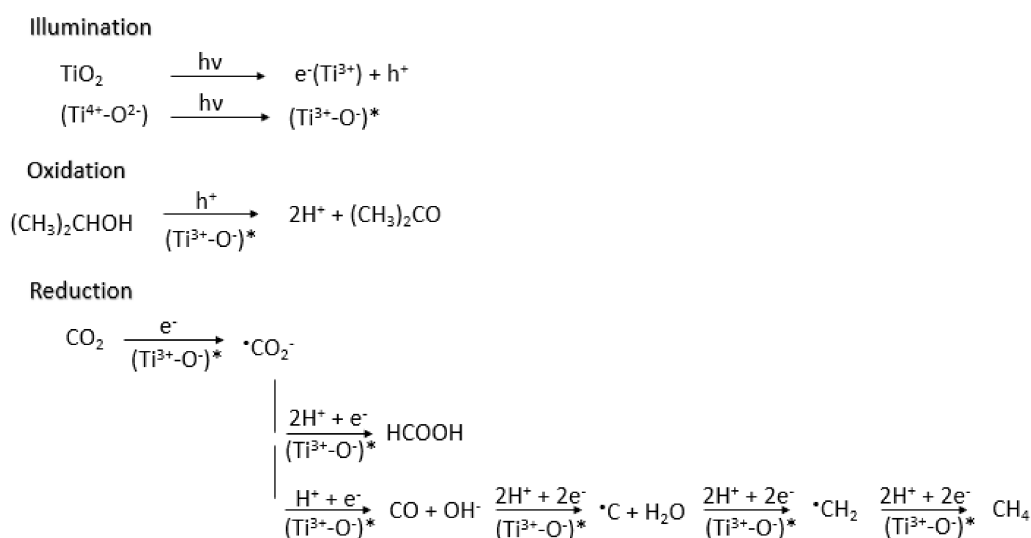
Illumination

$$TiO_2 \xrightarrow{h\nu} e^-(Ti^{3+}) + h^+$$

$$(Ti^{4+}\text{-}O^{2-}) \xrightarrow{h\nu} (Ti^{3+}\text{-}O^-)^*$$

Oxidation

$$(CH_3)_2CHOH \xrightarrow[(Ti^{3+}\text{-}O^-)^*]{h^+} 2H^+ + (CH_3)_2CO$$

Reduction

$$CO_2 \xrightarrow[(Ti^{3+}\text{-}O^-)^*]{e^-} {}^{\bullet}CO_2{}^-$$

$$\xrightarrow[(Ti^{3+}\text{-}O^-)^*]{2H^+ + e^-} HCOOH$$

$$\xrightarrow[(Ti^{3+}\text{-}O^-)^*]{H^+ + e^-} CO + OH^- \xrightarrow[(Ti^{3+}\text{-}O^-)^*]{2H^+ + 2e^-} {}^{\bullet}C + H_2O \xrightarrow[(Ti^{3+}\text{-}O^-)^*]{2H^+ + 2e^-} {}^{\bullet}CH_2 \xrightarrow[(Ti^{3+}\text{-}O^-)^*]{2H^+ + 2e^-} CH_4$$

Figure 4. Proposed mechanism of photocatalytic reduction of high-pressure CO_2 using TiO_2 and 2-propanol as a hole scavenger. Reproduced from [51], with permission from Elsevier, 1998.

Xia et al. synthesized a multi-walled carbon nanotube (MWCNT) supported TiO_2 and found that the addition of MWCNT greatly enhanced the photocatalytic activity of TiO_2 (Figure 5) [56]. As with other doped catalysts, it was found that there is an optimal amount of MWCNT before it begins to decrease the photocatalytic activity of TiO_2 due to the fact that excessive MWCNT can shield the TiO_2 from absorbing UV light. The optimal amount of MWCNT prevents TiO_2 from aggregating and can delay electron/hole recombination. Qin et al. made a bifunctionalized TiO_2 film containing a dye-sensitized zone and a catalysis zone designed for visible light photocatalytic CO_2 reduction (Figure 6) [57]. Electrons transferred from the dye to the conduction band of TiO_2 resulted in highly efficient conversion of CO_2 to formate, formaldehyde and methanol. After the electron injection, the dye is oxidized to dye$^+$, which can be regenerated by accepting electrons from I^- from the electrolyte. Ulagappan et al. studied the photoreduction of gaseous CO_2 in Ti-silicate molecular sieves using methanol as an electron donor [58]. The main result of the study is the detection of formate and it was proposed that upon excitation of the metal center, transient Ti^{+III} reduces CO_2 while methanol is oxidized.
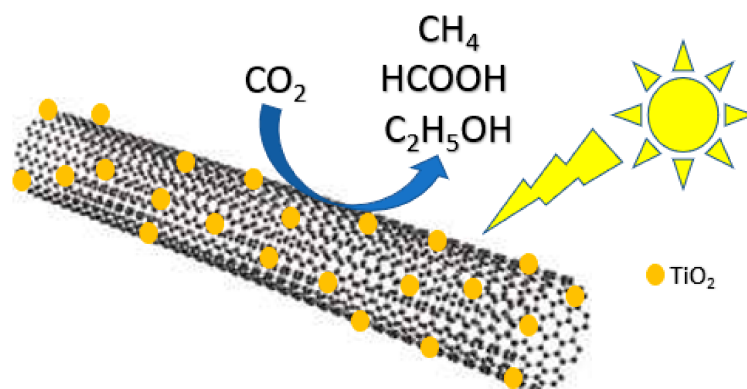

Figure 5. Photocatalytic CO_2 reduction to CH_4, HCOOH and C_2H_5OH using TiO_2-decorated multi-walled carbon nanotube (MWCNT).
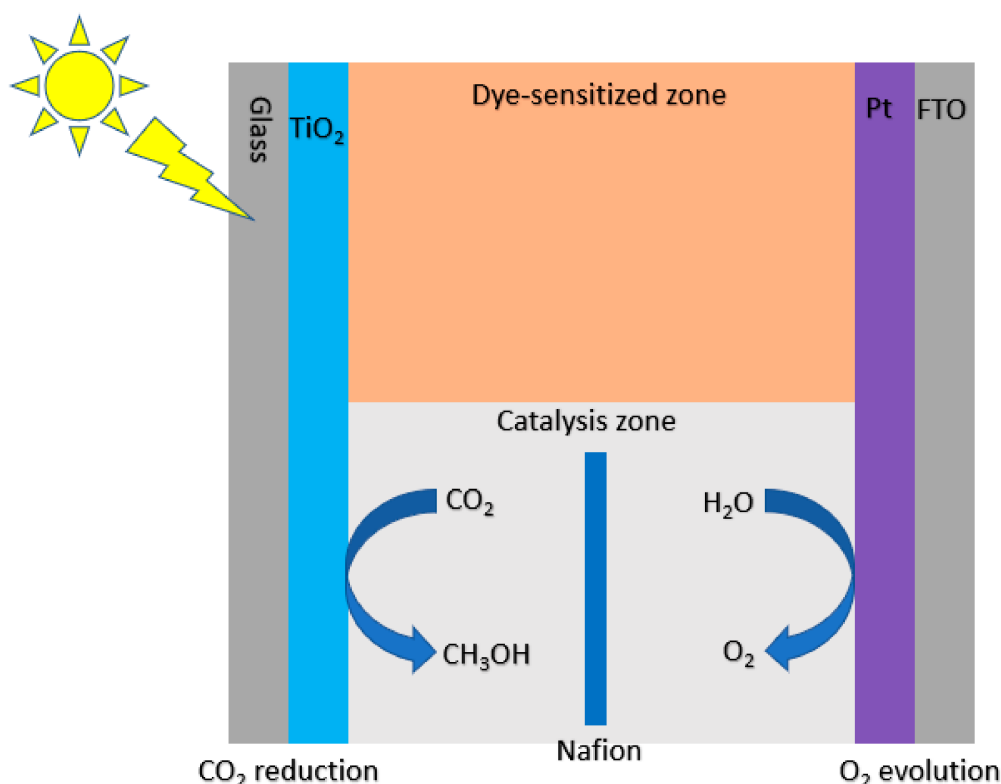
Figure 6. Proposed mechanism for the photocatalytic CO_2 reduction using bifunctionalized TiO_2 film.

In the 2000s, doping, co-catalyst and extending optical absorption to the visible region became a popular area for research. Sato et al. coupled a p-type semiconductor (N-doped Ta_2O_5) with a ruthenium complex as an electrocatalyst to produce formate from CO_2 [59]. This was the first report of electron transfer from semiconductor in the excited state to a metal complex in the ground state. Triethanolamine (TEOA) was used as an electron donor as well as a proton source and the measured quantum yield was 1.9% at 405 nm. A year later, Sato et al. studied the photoelectrochemical reduction of CO_2 over p-type InP/Ru complex polymer hybrid photocatalyst [60]. This reduction, using H_2O as an electron donor and proton source was achieved by using a two-step excitation process called a Z-scheme (Figure 7). Highly selective CO_2 photo-reduction was achieved by Arai and coworkers by combining Cu_2ZnSnS_4 (CZTS) with a metal complex electrocatalyst [61]. The main product was identified to be formate, which demonstrates the selectivity and efficiency of the hybrid semiconductor-metal-complex-electrocatalyst catalyst. Suzuki et al. continued on that idea of p-type photoactive N-doped Ti_2O_5 with a ruthenium complex, which can efficiently reduce CO_2 to formate using visible light [62].

Co-catalysts became a popular method to enhance semiconductor efficiency. Iizuka et al. used Ag as a co-catalyst for $ALa_4Ti_4O_{15}$ (where A = Ca, Sr and Ba) to reduce CO_2 to formate [63]. No sacrificial agent was used because water was consumed as a reducing agent (electron donor). It was found that the optimum Ag loading was 2 wt% and that $BaLa_4Ti_4O_{15}$ was the most active photocatalyst. Palladium is another noble metal that is often used as a co-catalyst. Raja et al. synthesized two photocatalysts-anodized titanium oxide nanotubes (T-NT) and bismuth titanate (BTO) decorated with palladium nanoparticles [64]. Pd-BTO showed a 2-fold increase in formic acid (110 μmol/h/g) yield when compared to bare BTO or T-NT, which is attributed to better charge separation in the hybrid Pd-BTO and the higher visible light harvesting ability of BTO because of its lower bandgap.
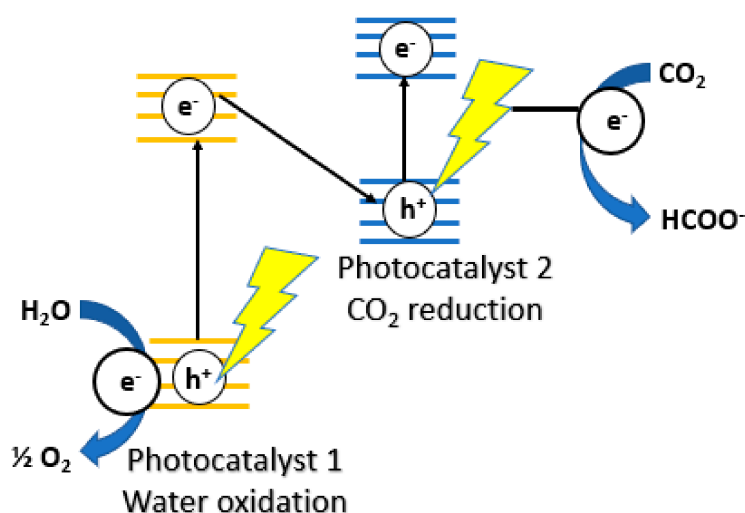
Figure 7. Illustration of the Z-scheme for CO_2 reduction. Reproduced from [60], with permission from American Chemical Society, 2011.

Mendoza et al. employed Co_3O_4 powders for CO_2 photo-reduction under visible light irradiation [65]. Co_3O_4 is a p-type semiconductor with band gap of 2.0 eV and has a conduction band edge that is more negative than the potentials of the CO_2 reduction reactions. In this study, formate was produced without any hole scavenger nor photo-sensitizer. Qin et al. synthesized a bismuth yttrium oxide ($BiYO_3$) photocatalyst for CO_2 reduction to formate under visible light irradiation [66]. Due to its large surface area and smaller band gap, $BiYO_3$ produced fewer hydroxyl radicals to give a higher formate yield.

Most recently, copper oxide and copper oxide-derivatives have been gaining attention as a highly active and earth abundant photocatalyst. Ali and coworkers designed a Z-scheme heterostructure composed of reduced titania and Cu_2O capable of reducing CO_2 to CH_4. Due to the Z-scheme architecture, Cu_2O was protected against photocorrosion and the photocatalyst was stable for 42 h. In addition, the synergistic interactions between reduced titania and Cu_2O resulted in 0.13% photoreduction of CO_2 to CH_4 [67]. Yin et al. grafted copper oxide nanoclusters onto niobate nanosheets, which served as a light harvesting component. This work found that photogenerated holes in the valence band of niobate nanosheets react with water and photogenerated electrons in the conduction band is injected into the copper oxide nanoclusters resulting in the production of carbon monoxide [68]. Lan et al. loaded Cu nanoparticles onto TiO_2 which exhibited significantly higher photocatalytic activity than pure TiO_2 for CO_2 reduction and selective for carbon monoxide [69]. Bae et al. synthesized zinc oxide-copper (I) oxide hybrid nanoparticles in colloidal forms with copper (I) oxide nanocubes bound to zinc oxide. This photocatalyst exhibited high selectivity for methane (>99%) which was attributed to the optimal band alignment of zinc oxide and copper (I) oxide, surface defects, high surface area and colloidal morphology of the catalyst [70]. Nogueira et al. evaluated the effect of electrolyte on photochemical CO_2 reduction using CuO nanoparticles and found electrolyte strongly influences product selectivity. NaOH led to methane production while $Na_2C_2O_4$ led to carbon monoxide production and $KBrO_3$ led to oxygen production [71]. Dedong et al. synthesized a Cu_2O/coal-based carbon nanoparticle hybrid to reduce CO_2 to methanol [72]. Zhang et al. fabricated an Ag-Cu_2O/ZnO nanorod hybrid catalyst and found Cu_2O enhances the CO_2 chemisorption on the catalyst surface while the formation of Z-scheme system between Cu_2O and ZnO facilitates charge separation. Silver nanoparticles onto Cu_2O leads to higher photocatalytic activity due to electron transfer from silver to Cu_2O [73]. Aguirre et al. found that TiO_2 can protect Cu_2O from undergoing photocorrosion when a Cu_2O/TiO_2 hybrid catalyst is formed. This hybrid creates an efficient Z-scheme which facilitates electron transfer from TiO_2 to Cu_2O [74]. Park et al. synthesized both CuO-TiO_2 and Cu_2O-TiO_2 and demonstrated this hybrid catalyst has enhanced light absorption and rapid charge

separation due to the intrinsic p-n heterojunction of the material, leading to improved photocatalytic activity [75]. Gusain et al. prepared reduced graphene oxide-copper oxide nanocomposites by covalent grafting of CuO nanorods onto reduced graphene oxide. Bare CuO showed low photocatalytic activity due to rapid charge carrier recombination but rGO-Cu_2O and rGO-CuO showed significantly higher photocatalytic activity in the reduction of CO_2 to methanol under visible light irradiation [76]. Zhai et al. synthesized a core-shell structure containing two co-catalysts capable of reducing CO_2 to methane and carbon monoxide. They propose that the Cu_2O shell provides sites for CO_2 reduction while the Pt core extracts photogenerated electrons from TiO_2 [77]. Wu et al. observed that the (110) facet of a single Cu_2O particle is capable of reducing CO_2 to methanol while the (100) facet is inert. The oxidation state of the active sites changes from Cu(I) to Cu(II) due to CO_2 and H_2O adsorption and changes back to Cu(I) after CO_2 conversion under visible light irradiation [78]. Table 2 summarizes the different types of semiconductors used in photocatalytic CO_2/bicarbonate reduction to formate and other products.

Table 2. Summary of CO_2 reduction using semiconductors.

Light Source	Reaction Medium and Electrolyte	Catalyst	Formate & Other Products	Ref.
Halogen lamp at 365 nm	Electrode consisting of single crystal GaP in 0.05 M K_2HPO_4/KH_2PO_4	GaP	HCOOH: 1.2×10^{-2} M HCHO: 3.2×10^{-4} M CH_3OH: 1.1×10^{-4} M	[33]
500 W Xe lamp	Aqueous Suspension of semiconductor in water	TiO_2, ZnO, CdS, GaP, SiC, WO_3	TiO_2: HCOOH: 1.8×10^{-3} M CH_3OH: 14.6×10^{-4} M ZnO: HCOOH: 1.2×10^{-3} M CH_3OH: 3.5×10^{-4} M CdS: HCOOH: 2.0×10^{-3} M CH_3OH: 11.7×10^{-4} M GaP: HCOOH: 1.0×10^{-3} M CH_3OH: 11.0×10^{-4} M SiC: HCOOH: 1.0×10^{-3} M CH_3OH: 53.5×10^{-4} M WO_3: HCOOH: 0 CH_3OH: 0	[34]
High pressure Hg lamp	Aqueous suspensions	Doped $BaTiO_3$, $LiNbO_3$	HCOOH and HCHO	[35]
150 W Xe lamp	Electrodes in 0.5 M Na_2CO_3	Single crystal p-GaP, p-GaAs	p-GaP: HCOOH: 670 µmol HCHO: 13 µmol CH_3OH: 10 µmol p-GaAs: HCOOH: 320 µmol HCHO: 5 µmol	[36]
High pressure Hg lamp	Aqueous suspension in water	RuO_2-doped TiO_2	HCOOH: 1.46 µmol/h HCHO: 0.18 µmol/h CH_3OH: 0.2 µmol/h	[37]
High pressure Hg lamp	Aqueous suspension in 1.5×10^{-3} M $NaHCO_3$	Cd-loaded ZnS	Quantum efficiency: HCOOH: 32.5% HCHO: 42.0% H_2: 5.0%	[38]
High pressure Hg lamp	Colloidal suspension in 0.7 M NaH_2PO_2	ZnS	HCOOH: 75.1 µmol/h CO: 2.7 µmol/h H_2: 86.0 µmol/h	[39]
Tungsten-halogen lamp ($\lambda > 350$ nm)	Aqueous suspension in water	ZnS-loaded SiO_2	HCOOH: 10 mmol	[40]
1000 W Xenon arc lamp	Aqueous suspension in 0.2 M $NaHCO_3$	ZnS	HCOOH: 140 mmol formate/g cat-hr	[20]
1000 W Xenon arc lamp	Aqueous suspension in 0.2 M $NaHCO_3$	Cu_2O	HCOOH: 2.78 mmol formate/g cat-hr	[41]
1000 W Xenon arc lamp	Aqueous suspension in 0.2 M $NaHCO_3$	Au/TiO_2	HCOOH: 55 mmol formate/g cat-hr	[42]
1000 W Xenon arc lamp	Aqueous suspension in 0.2 M $NaHCO_3$	Ag/TiO_2	HCOOH: 3.89 mmol formate/g cat-hr	[43]
1000 W Xenon arc lamp	Aqueous suspension in 0.2 M $NaHCO_3$	TiN/TiO_2	HCOOH: 3000 mmol formate/g cat-hr	[44]

Table 2. *Cont.*

Light Source	Reaction Medium and Electrolyte	Catalyst	Formate & Other Products	Ref.
150 W XBO arc lamp	Aqueous suspension in water	Ru nanoparticles-loaded ZnS	HCOOH:0.006 M	[45]
High pressure Hg lamp	Colloidal suspension in H_3PO_4	ZnS microcrystallite	HCOOH: 11.6 µmol HCHO: 11.8 µmol CH_3OH: 1.2 µmol	[46]
Medium pressure mercury lamp	Aqueous suspension in water	CdS, ZnO, SiC, Ba TiO_3, $SrTiO_3$	HCOOH, HCHO	[47]
Medium pressure mercury lamp	Aqueous suspension in water	CdS, ZnS	ZnS: HCOOH: 320 µmol/L CdS: HCOOH: 87 µmol/L	[48]
Medium pressure mercury lamp	Aqueous suspension in water	SiO_2-stabilized ZnS	HCOOH: 0.8% AQE	[49]
990 W Xe lamp	Aqueous suspension in water	TiO_2	HCOOH: 8×10^{-6} mol/g-cat	[50]
Xe lamp	Aqueous suspension in water	TiO_2	HCOOH: 2.3×10^{-6} mol/g-cat CH_4: 1.2×10^{-6} mol/g-cat	[51]
990 W Xe lamp	Power in supercritical fluid CO_2	TiO_2	HCOOH: 9×10^{-6} mol/g-cat	[52]
500 W high pressure mercury arc lamp	Aqueous suspension in water and 2-propanol	CdS	HCOOH: 0.4 µmol HCHO: 1.9 µmol CO: 0.8 µmol H_2: 0.5 µmol	[53]
100 W tungsten halogen lamp, 150 W xenon lamp	Aqueous suspension in water	CdS-SiO_2, CdS-ZnS	CdS-SiO_2: HCOOH: 10×10^{-5} M HCHO: 3.4×10^{-5} M CdS-ZnS: HCOOH: 4.5×10^{-5} M	[54]
450 W medium pressure UV Hg arc lamp	Aqueous suspension in water and 7.2 mM NaHS and 2.5 mM $NaHCO_3$	MnS	HCOOH: 200 µM	[55]
15 W UV lamp $\lambda = 365$ nm	Aqueous suspension in water	MWCNT-supported TiO_2	HCOOH: 125.1 µmol/g CH_4: 73.33 µmol/g C_2H_5OH: 149.36 µmol/g	[56]
300 W Xe lamp	Electrode in water adjusted to pH 4	Dye-sensitized TiO_2 film	HCOOH: 1.8 mmol/cm^2 HCHO: 1.4 mmol/cm^2 CH_3OH: 1.9 mmol/cm^2	[57]
Pulsed Nd:YAG laser at 10 Hz, $\lambda = 266$ nm	Methanol	Ti silicalite molecular sieve	HCOOH, CO	[58]
Xe lamp	Aqueous suspension in MeCN/TEOA	N-doped Ta_2O_5 (N-Ta_2O_5), linked with electrocatalysts [Ru(dcbpy)(bpy)(CO)$_2$]$^{2+}$ or [Ru-(dcbpy)$_2$(CO)$_2$]$^{2+}$	HCOOH: 1.9% quantum yield	[59]
Solar simulator with AM 1.5 filter	Aqueous suspension in water and 10 mM $NaHCO_3$	InP/Ru complex polymer hybrid	HCOOH: 4.71 µmol/cm^2	[60]
Xe light source	Aqueous suspension in water	Cu_2ZnSnS_4	HCOOH: 0.22 mM	[61]
500 W Xe lamp	Aqueous suspension in acetonitrile/triethanolamine	N-doped Ta_2O_5 with [Ru(dcbpy)$_2$(CO)$_2$]$^{2+}$	HCOOH: 1.9 quantum efficiency	[62]
400 W high-pressure mercury lamp	Aqueous suspension in water	Ag-loaded $ALa_4Ti_4O_{15}$ (A = Ca, Sr, Ba)	$BaLa_4Ti_4O_{15}$: HCOOH: 150 µmol	[63]

Table 2. *Cont.*

Light Source	Reaction Medium and Electrolyte	Catalyst	Formate & Other Products	Ref.
300 W solar simulator with AM 1.5 filter	Thin films submerged in 0.1 M H_2SO_4	Anodized titanium oxide nanotubes (T-NT), Pd-decorated bismuth titanate (BTO)	HCOOH: 160 µmol/h/g	[64]
21 W LED lamp, λ = 510 to 620 nm	Aqueous suspension in water	Co_3O_4	HCOOH: 4.53 µmol/g-h HCHO: 0.62 µmol/g-h	[65]
300 W Xe lamp	Aqueous suspension in 0.25 M NaOH and 0.1 M Na_2SO_3	$BiYO_3$	HCOOH: 1.68 µmol/L	[66]
100W solar simulator with AM 1.5 filter	CO_2 passing through solid photocatalyst	Reduced titania-Cu_2O	CH_4: 462 nmol/g	[67]
Xe–Hg lamp	Aqueous suspension in 0.5 M $KHCO_3$	Cu(II)-grafted $Nb_3O_8^-$ nanosheets	CO: 1.5 µmol	[68]
300 W Xe lamp	Aqueous suspension in water	Cu-TiO_2	CO: 244 µmol/g	[69]
300 W Xe lamp	Aqueous suspension in water and 0.2 M Na_2CO_3	ZnO-Cu_2O nanoparticles	CH4: 1080 µmol/g_{cat} h CO: 1.4 µmol/g_{cat} h	[70]
5 W UVC lamp	Aqueous suspension in 0.1 M $Na_2C_2O_4$, 0.1 M $KBrO_3$, 0.1 M NaOH or water	CuO	CH4: 1000 µmol/L-g CO: 6 µmol/L-g	[71]
300 W Xenon lamp	Aqueous suspension in 1M NaOH	Cu_2O/CNPs	CH_3OH: 236.43µmolg^{-1}cat	[72]
300 W Xe arc lamp	Aqueous suspension in water	Ag-Cu_2O/ZnO nanorods	CO: 9.94 µmol/g	[73]
1 kW high-pressure Hg (Xe) arc lamp	Aqueous suspension in water	Cu_2O/TiO_2	CO: 2.11 µmol g_{cat}^{-1} h^{-1}	[74]
100 W Xenon solar simulator with AM 1.5 filter	Powder photocatalyst with CO_2	Cu_xO-TiO_2	CH4: 221.6 ppm/g-h	[75]
20 W white cold LED flood light	Aqueous suspension in DMF and water	rGO-CuO, rGO-Cu_2O	rGO-CuO: CH_3OH: 1228 µmol/g rGO-Cu_2O: CH_3OH: 862 µmol/g	[76]
200 W Xe lamp	Powder photocatalyst with CO_2	TiO_2-loaded Pt and Cu	Pt/TiO_2: CH_4: 11 µmol/g-h CO: 2.2 µmol/g-h Cu/TiO_2: CH_4: 8.7 µmol/g-h CO: 5.4 µmol/g-h Pt-Cu/TiO_2: CH_4: 9.8 µmol/g-h CO: 5.9 µmol/g-h	[77]
300 W Xe lamp	Aqueous suspension in water	Cu_2O	CH_3OH: 1.2 mol g^{-1} h^{-1}	[78]

4.2. Phthalocyanine-Semiconductor Composites

Phthalocyanines are macrocyclic heterostructures with aromatic conjugated complexes consisting of nitrogen and carbon atoms. They offer enormous potential as the light harvesting components of dye-sensitized semiconductors [79]. They also offer high photo and thermal stability and low toxicity. In addition, the close position of the TiO_2 conduction band with respect to the LUMO orbital energy of the phthalocyanines favors efficient charge transfer. When the phthalocyanines molecule is excited by visible light, electrons are excited from the HOMO to the LUMO energy level and is then injected into the conduction band of TiO_2.

In 1997, Premkumar et al. was able to produce formate from carbon dioxide upon photo-reduction by metal phthalocyanines (cobalt and zinc) adsorbed onto a Nafion membrane that acted as a

photocatalyst in acidic aqueous solution containing triethanolamine as a hole scavenger [80,81]. The catalyst was immobilized in the Nafion membrane and because they are physically separated from the solution phase they are able to exhibit high photocatalytic efficiency (Figure 8). It was found that the membranes behave as a p-type semiconductor and high turnover numbers were achieved. In 2009, Liu et al. synthesized CoPc-loaded TiO_2 and in the presence of NaOH, produced high formate yield [82]. Na_2SO_3 was used as a hole scavenger and under optimal conditions, 1032 µmol/g cat of formate was produced. It was found that with the addition of CoPc, formate production significantly increased, with optimal CoPc loading being 0.5 wt%. The contact of TiO_2 and CoPc involves redistribution of charge. Because the oxidation potential of S_1 of CoPc is higher than the conduction band of TiO_2, while the energy of T_1 is lower than the conduction band of TiO_2 (Figure 9), it is thermodynamically feasible for electron transfer from CoPc to TiO_2. When this occurs, CoPc is oxidized to $CoPc^{*+}$. The influence of NaOH, hole scavenger and irradiation time has been investigated. Because NaOH can dissolve more CO_2 than pure water, making HCO_3^- the predominant form in aqueous solution therefore accelerating the photoreduction [82]. The mechanism of CO_2 reduction with CoPc-loaded TiO_2 begins with photo-excitation of the CoPc from S_0 to S_1, which can subsequently transfer its electrons to the conduction band of TiO_2. CO_2 molecules adsorbed onto the surface of TiO_2 gain electrons and are reduced (Equations (10) and (11)) [81].

$$CoPc\ (S_0) + h\upsilon \rightarrow CoPc^*(S_1) \tag{10}$$

$$CoPc^*(S_1) + TiO_2(CB) \rightarrow CoPc^{\bullet+} + e^-(TiO_2/CB). \tag{11}$$
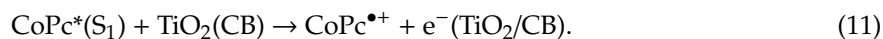
In 2009, Zhao et al. also synthesized a $CoPc/TiO_2$ nanocomposite to reduce CO_2 under visible light irradiation [83]. CoPc molecules are excited first and are able to inject their electrons into TiO_2, this allows for the increased separation of electron/hole pairs and thus increasing the photocatalytic efficiency to 1714 µmol/g cat. In 2013, Yazdanpour et al. synthesized copper phthalocyanine-modified TiO_2 ($CuPc/TiO_2$), which was coated on a stainless steel mesh and used for the photo-reduction of CO_2 in the presence of visible light [84]. Mele et al. synthesized copper and zinc phthalocyanine-loaded TiO_2 under visible light irradiation [79]. They reported that $CuPc/TiO_2$ was the most efficient yielding formate production of 208.5 µmol/g cat. In 2015, Mele expanded on their work of CuPc-loaded TiO_2 by studying both Cu(II) porphyrin and Cu(II) phthalocyanine loaded onto TiO_2 [85]. Cu(II) phthalocyanine-loaded TiO_2 was more efficient in the photoreduction of CO_2 to formate due to its favorable reduction potential. This work reported a detailed study of the effect of the amount of catalyst, initial pH, copper loading in the $CuPc-TiO_2$ composite, irradiation source and sensitizers. This work reported production values for formate of 239.5 µmol/g cat. Table 3 summarizes various phthalocyanine-enhanced semiconductors to reduce CO_2/bicarbonate to formate and other products.
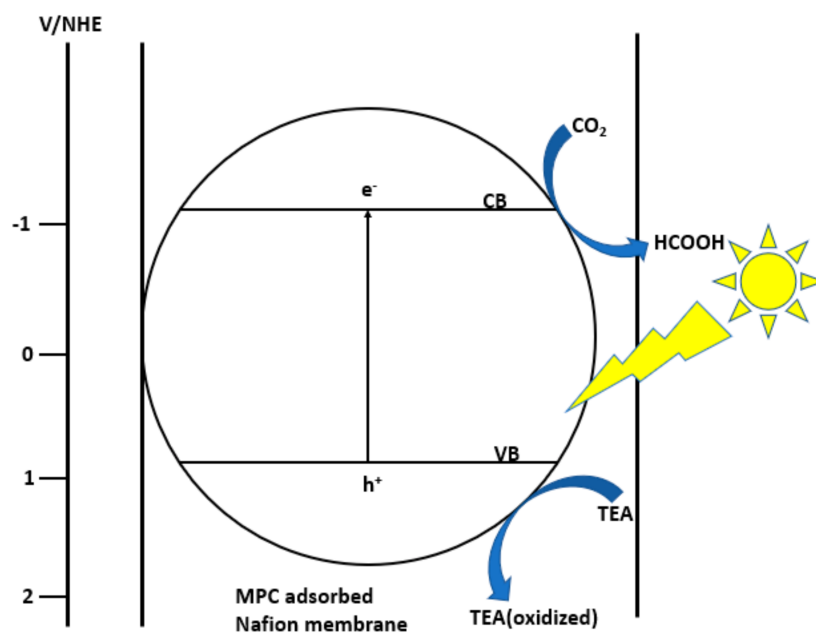
Figure 8. Schematic illustration of the photocatalytic CO_2 reduction at MPC adsorbed in a Nafion membrane. (Circle represents the semiconducting nature of the adsorbed MPC Nafion membrane. MPC = CoPC or ZnPC, TEA = triethanolamine, CB = conduction band, VB = valence band and EF = Fermi level).
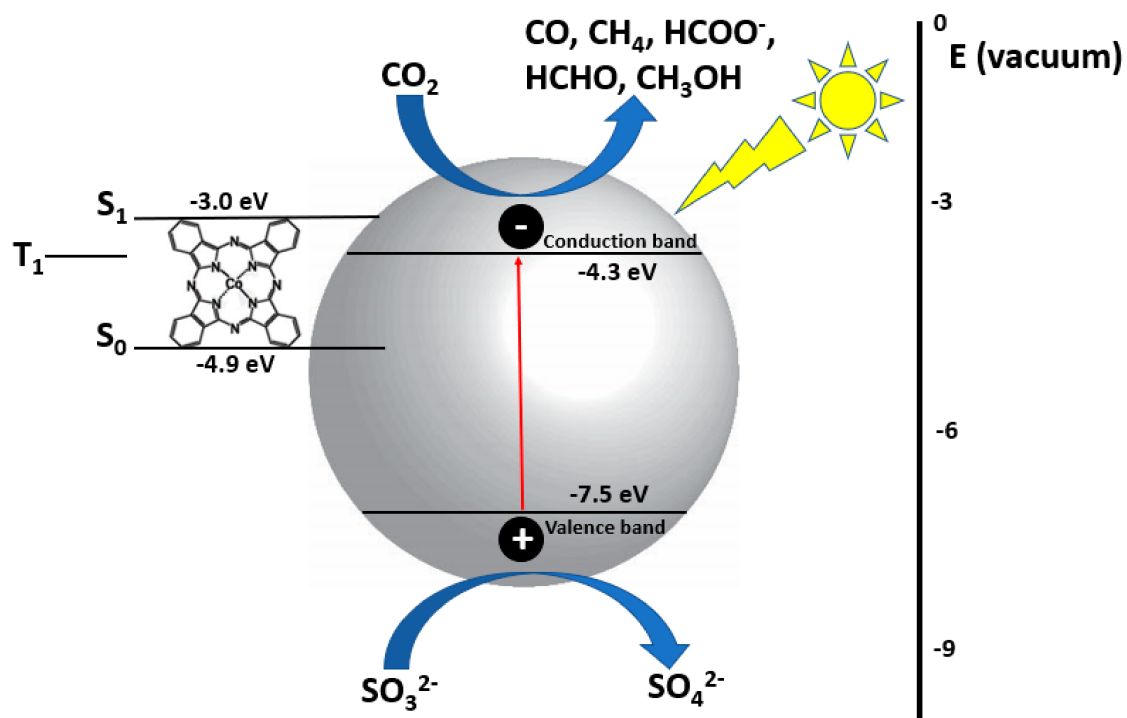

Figure 9. Photocatalytic CO_2 reduction using CoPc-loaded TiO_2.

Table 3. Summary of CO_2 reduction using phthalocyanines.

Light Source	Reaction Medium and Electrolyte	Catalyst	Formate & Other Products	Ref.
300 UV-VIS UV-VIS lamp and 400 W Xe-Halogen lamp S: SANOLIUX HRC uv vis lamp 300 W H: RADIUM Xe-Halogen lamp 400 W	Aqueous suspension in water, pH adjusted by NaOH or H_3PO_4	Lipophilic phthalocyanines/ TiO_2 composites	Product yield in µmol/g cat TiO_2 with pH 3 and a S/H light source: 131 HCOOH TiO_2-H_2Pc with pH 3 and a S/H light source: 75 HCOOH TiO_2-CuPc with pH 3 and a S/H light source: 208.5 HCOOH TiO_2-ZnPc with pH 3 and a S/H light source: 88.5 HCOOH TiO_2-CuPc with pH 7 and a S/H light source: 63.4 HCOOH TiO_2-CuPc with pH 13 and a S/H light source: 65.2 HCOOH TiO_2-CuPc with pH 3 and a S light source: 32.6 HCOOH TiO_2-CuPc with pH 3 and a H light source: 52.2 HCOOH	[79]
500 W tungsten-halogen lamp	Membrane dipped in water with 0.1 M TEA and 0.1 M $HClO_4$	MP-Nafion, MPC-Nafion	Nf/PP: 8×10^{-5} mol Nf/CoTPP: 2.9×10^{-4} mol Nf/FePC: 11×10^{-5} mol Nf/ZnPC: 2×10^{-4} mol	[80]
500 W tungsten–halogen lamp	Membrane dipped in 0.1 M triethanolamine and 0.1 M $HClO_4$	MPC-Nafion	Nf-CoPc: 1.7×10^4 mol Nf-ZnPc: 2.0×10^4 mol	[81]
500 W tungsten–halogen lamp	Aqueous suspension in NaOH	CoPc-TiO_2	With 0 [HCHO]/M and 0 [CH_3OH]/M: HCOOH: 289.9 µmol/(g cat) With 0 [HCHO]/M and 0.5 [CH_3OH]/M: HCOOH: 292.8 µmol/(g cat) With 0 [HCHO]/M and 5 [CH_3OH]/M: HCOOH: 301.1 µmol/(g cat) With 0.1 [HCHO]/M and 0 [CH_3OH]/M: HCOOH: 9731.3 µmol/(g cat) With 1 [HCHO]/M and 0 [CH_3OH]/M: HCOOH: 82660.5 µmol/(g cat)	[82]
500 W tungsten-halogen lamp	Aqueous suspension in 0.1 N NaOH	CoPc-TiO_2	1.0 wt% CoPc/TiO_2: HCOOH: 450.6 µmol/g cat 0.7 wt% In-situ CoPc/TiO_2: HCOOH: 1487.6 µmol/g cat	[83]
125 W high pressure mercury lamp	CO_2 passed through catalyst-coasted reaction vessel	CuPc-TiO_2	14% photoconversion	[84]
300 UV-VIS UV-VIS lamp and 400 W Xe-Halogen lamp	Aqueous suspension in water, pH adjusted by NaOH or H_3PO_4	CuPc-TiO_2	HCOOH: 239.5 µmol/gcat	[85]

4.3. Metal-Organic Frameworks

Metal-organic frameworks (MOFs) are a class of crystalline materials made by joining metal ions or clusters and organic linkers together. Inorganic metals are called secondary building units (SBU) and organic units are ditopic or polytopic organic carboxylates. The different combinations of organic and inorganic components, as well as varying the geometry, size and functionality has led to more than 20,000 different MOFs being synthesized [86]. The three most distinguishing features of MOFs are their large surface area and ultrahigh porosity; as well as its permanent porosity. MOFs are stable structures that do not collapse upon the removal of solvent. Compared to commercial TiO_2 (P-25) that have surface area of only 35–65 m^2/g, MOFs have a tremendous amount of surface area. Surface area of MOFs typically range from 1000 to 10,000 m^2/g and their porosity is greater than 50% of the MOF crystal volume [86]. MOFs are also shown to be thermally and chemically stable. It is these properties of MOFs that give them a great advantage over other porous materials such as zeolites and carbon-based materials.

Metal-organic frameworks (MOFs) are emerging as a new type of promising photocatalysts. MOFs are a class of crystalline and microporous material with a vast array of topologies and applications in numerous fields such as gas sensing, catalysis, gas storage and separation and drug delivery [87]. In MOFs the metal clusters can be regarded as inorganic semiconductor quantum dots that are linked by organic linkers serving as antennas to activate the quantum dots [88]. Electron injections occurs from the photo-excited organic linkers to the metal clusters, termed linker-to-cluster charge transfer (LCCT). MOFs are superior to semiconductors because their light absorption ability can be easily tuned

by modifications on the organic linkers to make them visible-light responsive [89]. Table 4 summarizes CO_2 reduction using various metal-organic frameworks.

Table 4. Summary of CO_2 reduction using metal-organic frameworks.

Light Source	Reaction Medium and Electrolyte	Catalyst	Formate & Other Products	Ref.
500 W Xe lamp	Aqueous suspension in 5:1 ratio of MeCN and TEOA	NH$_2$-Uio-66(Zr)	NH$_2$-Uio-66(Zr): HCOOH: 13.2 μmol in 10 h Mixed NH$_2$-Uio-66(Zr): HCOOH:20.7 μmol in 10 h NH$_2$-UiO-66(Zr): HCOOH: None Mixed NH$_2$-UiO-66(Zr): HCOOH:7.28 μmol	[88]
300 W Xe lamp	Aqueous suspension in 5:1 ratio of MeCN and TEOA	MIL-101 (Fe), MIL-53 (Fe), MIL-88B (Fe),	NH$_2$-MIL-101(Fe): HCOOH: 178 μmol MIL-101(Fe): HCOOH: 59.0 μmol NH$_2$-MIL-53(Fe): HCOOH: 46.5 μmol MIL-53(FE): HCOOH: 29.7 μmol NH$_2$-MIL-88(Fe): HCOOH: 30.0 μmol MIL-88(Fe): HCOOH: 9.0 μmol	[89]
500 W Xe lamp	Aqueous suspension in 5:1 ratio of MeCN and TEOA	NH$_2$-MIL-125(Ti)	NH$_2$-MIL-125(Ti): HCOOH: 8.14 μmol NH$_2$-MIL-125(Ti) (λ > 450 nm): HCOOH: 3.83 μmol	[90]
470 nm LED	Aqueous suspension in 4:1 ratio of DMF/TEOA solvent mixture containing 0.2 M 1-benzyl-1,4-dihydronicotiamide (BNAH)	Mn(bpydc)(CO)$_3$Br incorporated into Zr(IV)-based metal−organic framework	Turnover numbers for Products: UiO-67-Mn(bpy)(CO)$_3$Br(b) for 4 h: HCOOH: 50 UiO-67-Mn(bpy)(CO)$_3$Br(b) for 18 h: HCOOH: 110	[91]
300 W Xe arc lamp	Aqueous suspension in 4:1 mixed solution of acetonitrile (MeCN)-triethanolamine (TEOA), which contained 1-benzyl-1,4-dihydronicotiamide (0.1 M, BNAH)	Zr$_{4.3}$Ti$_{1.7}$O$_4$(OH)$_4$(C$_8$H$_7$O$_4$N)$_{5.17}$(C$_8$H$_8$O$_4$N$_2$)$_{0.83}$	Zr$_{4.3}$Ti$_{1.7}$O$_4$(OH)$_4$(C$_8$H$_7$O$_4$N)$_{5.17}$(C$_8$H$_8$O$_4$N$_2$)$_{0.83}$: HCOOH: 31.57 μmol UiO-66(Zr/Ti)-NH$_2$: HCOOH: 4.66 μmol	[92]

Fu et al. synthesized a Ti-based MOF Ti$_8$O$_8$(OH)$_4$(BDC)$_6$ (where BCD = benzene-1,4-dicarboxylate) and the photocatalytic reduction of CO_2 was performed in acetonitrile with triethanolamine (TEOA) as a sacrificial agent under visible light irradiation [90]. This MOF exhibited extremely high surface area of 1302 m^2/g that produced 8.14 μmol of formate after 10 h. Upon irradiation in the LMCT band, a long-lived excited charge separate state occurs by transferring an electron from the organic ligand to Ti^{4+} (Figure 10). Sun et al. synthesized NH$_2$-UiO-66(Zr), which is a Zr-containing MOF composed of hexameric Zr$_6$O$_{32}$ units linked by benzenedicarboxylate (BDC) [88]. This study substituted the BDC ligand with 2-aminoterephthalic acid (ATA), which rendered the MOF visible-light responsive due to the amino substituent. In the presence of triethanolamine as a sacrificial agent, visible light irradiation was able to reduce CO_2 to formate reaching production values of 20.7 μmol/g cat-hr. Wang et al. reported synthesizing a series of earth-abundant Fe-containing MOFs that are able to reduce CO_2 under visible light irradiation [89]. The direct excitation of the Fe-O clusters induces the electron transfer from O^{2-} to Fe^{3+} to form Fe^{2+}, which is responsible for the CO_2 reduction. In addition, when these MOFs are functionalized with an amine substituent, their catalytic efficiency is greatly increased. This is attributed to the existence of dual excitation pathways: excitation of the NH$_2$ functionality is followed by electron transfer to the Fe center and the direct excitation of Fe-O clusters. In the presence of TEOA as a sacrificial agent, formate production reached 178 μmol. Fei et al. incorporated a manganese bipyridine complex [Mn(bpydc)-(CO)$_3$Br] into a robust Zr(IV)-based MOF for CO_2 reduction to formate [91]. [Ru(dmb)$_3$]$^{2+}$ was used as a photosensitizer and 1-benzyl-1,4-dihydronicotinamide (BNAH) was used as a sacrificial agent (Figure 11). The enhanced photocatalytic efficiency was ascribed to the structure of the framework providing isolated active sites, which stabilize the catalyst. The catalyst maintained its crystallinity and was reused over several runs. Most recently, Lee et al. synthesized a mixed metal (Zr/Ti) MOF to reduce CO_2 to formate under visible light irradiation [92]. TEOA was used as a sacrificial base and 1-benzyl-1,4-dihydronicotinamide (BNAH) as a sacrificial reductant. The MOFs

were studied by photoluminescence spectroscopy to study charge transfer from organic linker to the metal cluster. This work resulted in high turnover numbers and the catalysts were recyclable over three runs.
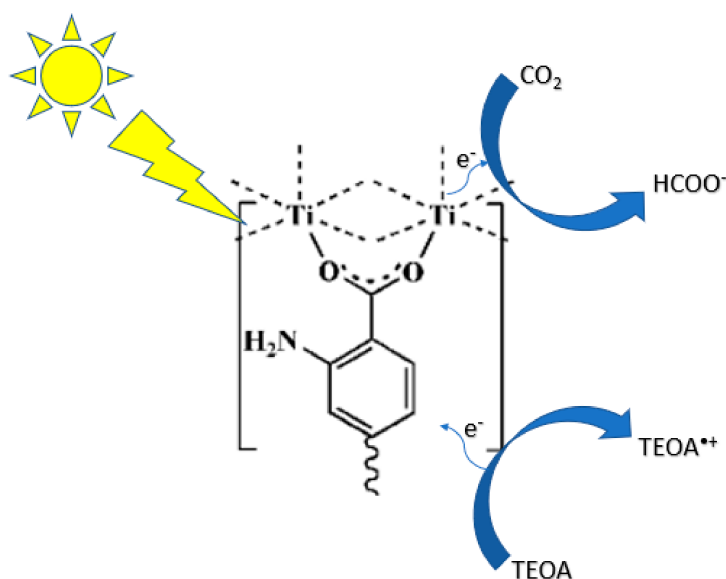
Figure 10. Proposed mechanism for the photocatalytic CO_2 reduction using NH_2-MIL-125(Ti) under visible light irradiation.
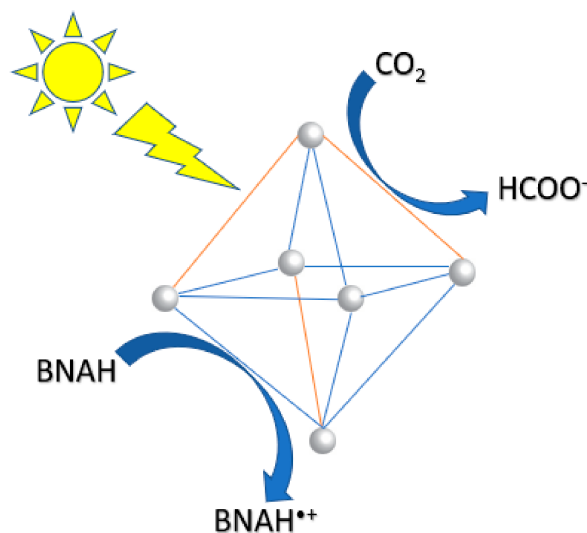
Figure 11. Proposed mechanism for photocatalytic formate production using UiO-67-Mn(bpy)(CO)$_3$Br.

5. Future Perspectives and Outlook

The majority of this review is focused on semiconductors for CO_2/bicarbonate reduction because they are the most widely used photocatalyst. However, quantum efficiencies are still low due to extremely rapid electron/hole recombination within the semiconductor, narrow optical absorption of the semiconductor, scattering of the semiconductor, competing hydrogen evolution reaction and products getting re-oxidized to CO_2. Though these issues can be mitigated by using photosensitizers and hole scavengers, a lot of work still needs to be done to make the reaction more efficient. In addition, semiconductors eventually degrade over time, so more durable catalysts need to be designed. Plasmon-enhanced photocatalysis is a rapidly expanding field due to the excellent optical properties of plasmonic noble-metal nanoparticles such as Au and Ag. Plasmonic nanoparticles

primarily absorb in the visible region of the solar spectrum and are known to generate hot electrons that can be injected into the conduction band of semiconductors, allowing for excess electrons available for reduction. Plasmonic nanoparticles, along with organic dyes, can act as excellent photosensitizers for semiconductors.

Moving forward, design strategies for photocatalysts include the fabrication of three-dimensional hierarchical nanostructures to maximize surface area, catalyst kinks and defects and grain boundaries to allow for molecular adsorption to the catalyst surface. Different metal crystal structures and surface facets lead to different product distribution, therefore tuning the metal surface structure will allow for precise control over product selectivity. The addition of photosensitizers to render a catalyst visible light-responsive will maximize the region of optical absorption and the ability to utilize more of the solar spectrum. With these techniques, rational design of efficient, selective and durable catalysts is possible. With the development of these catalysts, one can then scale up and design reactors that can convert CO_2 or flue gas into value-added products.

6. Conclusions

In conclusion, many significant achievements have been made in the field of photocatalytic CO_2 reduction. In relation to hydrogen production, which remains an impactful renewable energy source, the case is made for the chemical conversion of CO_2 to formate in terms of near term economic feasibility and in juxtaposition to geological storage and sequestration. Based on this review, one can see that the majority of photocatalysts for CO_2 reduction to formate are comprised of semiconductors. However, due to their narrow region of optical absorption, many studies have incorporated ruthenium complexes, phthalocyanines, and employed metal-organic framework catalysts designed to be visible-light responsive. Other catalysts include the use of graphene and graphene oxide as electron sinks to improve charge separation. Albeit much effort has been put into studying CO_2 reduction, the photoconversion efficiency and selectivity for desired products is still low. The mechanism of CO_2 reduction still needs to be investigated in depth. The one-electron induced activation of CO_2 into the anion radical $CO_2^{\bullet-}$ still requires a high overpotential, which seems to be the rate-limiting step. The development of photocatalytic materials for CO_2 reduction is rapidly expanding and will continue to reach higher efficiencies. As apparent quantum efficiencies improve with current research trends and new investigators entering the field, we assert that more practical device and design will become a major research component to the success of greenhouse gas mitigation and regenerative energy.

References

1. Barber, J. Photosynthetic energy conversion: Natural and artificial. *Chem. Soc. Rev.* **2009**, *38*, 185–196. [CrossRef] [PubMed]
2. Sayigh, A. *Comprehensive Renewable Energy*; Elsevier: Amsterdam, The Netherlands, 2012.
3. Hammarström, L.; Hammes-Schiffer, S. Artificial photosynthesis and solar fuels. *Acc. Chem. Res.* **2009**, *42*, 1859–1860. [CrossRef] [PubMed]
4. British Petroleum (BP). *Statistical Review of World Energy*; BP plc: London, UK, 2020.
5. Kannan, N.; Vakeesan, D. Solar energy for future world—A review. *Renew. Sustain. Energy Rev.* **2016**, *62*, 1092–1105. [CrossRef]
6. Olah, G.A.; Goeppert, A.; Surya Prakash, G.K. *Beyond Oil and Gas: The Methanol Economy*; Wiley-VCH: Weinheim, Germany, 2006.

7. Olah, G.A.; Mathew, T.; Goeppert, A.; Surya Prakash, G.K. Difference and significance of regenerative vs. renewable carbon fuels and products. *Top. Catal.* **2018**, *61*, 522–529. [CrossRef]

8. Yue, D.; You, F.; Snyder, S.W. Biomass-to-bioenergy and biofuel supply chain optimization: Overview, key issues and challenges. *Comput. Chem. Eng.* **2014**, *66*, 36–56. [CrossRef]

9. Habisreutinger, S.N.; Schmidt-Mende, L.; Stolarczyk, J.K. Photocatalytic Reduction of CO_2 on TiO_2 and Other Semiconductors. *Angew. Chem. Int. Ed.* **2013**, *52*, 7372–7408. [CrossRef]

10. Windle, C.D.; Perutz, R.N. Advances in molecular photocatalytic and electrocatalytic CO_2 reduction. *Coord. Chem. Rev.* **2012**, *256*, 2562–2570. [CrossRef]

11. Nitopi, S.; Bertheussen, E.; Scott, S.B.; Liu, X.; Engstfeld, A.K.; Horch, S.; Seger, B.; Stephens, I.E.L.; Chan, K.; Hahn, C.; et al. Progress and perspectives of electrochemical CO_2 reduction on copper in aqueous electrolyte. *Chem. Rev.* **2019**, *119*, 7610–7672. [CrossRef]

12. Lee, M.-Y.; Park, K.T.; Lee, W.; Lim, H.; Kwon, Y.; Kang, S. Current achievements and the future direction of electrochemical CO_2 reduction: A short review. *Crit. Rev. Environ. Sci. Technol.* **2020**, *50*, 769–815. [CrossRef]

13. Chang, X.; Wang, T.; Gong, J. CO_2 photo-reduction: Insights into CO_2 activation and reaction on surfaces of photocatalysts. *Energy Environ. Sci.* **2016**, *9*, 2177–2196. [CrossRef]

14. Morris, A.J.; Meyer, G.J.; Fujita, E. Molecular approaches to the photocatalytic reduction of carbon dioxide for solar fuels. *Acc. Chem. Res.* **2009**, *42*, 1983–1994. [CrossRef] [PubMed]

15. Hong, J.; Zhang, W.; Ren, J.; Xu, R. Photocatalytic reduction of CO_2: A brief review on product analysis and systematic methods. *Anal. Methods* **2013**, *5*, 1086–1097. [CrossRef]

16. Xie, S.; Zhang, Q.; Liu, G.; Wang, Y. Photocatalytic and photoelectrocatalytic reduction of CO_2 using heterogeneous catalysts with controlled nanostructures. *Chem. Commun.* **2016**, *52*, 35–59. [CrossRef] [PubMed]

17. Kumar, B.; Llorente, M.; Froehlich, J.; Dang, T.; Sathrum, A.; Kubiak, C.P. Photochemical and Photoelectrochemical Reduction of CO_2. *Annu. Rev. Phys. Chem.* **2012**, *63*, 541–569. [CrossRef]

18. Song, C. Global challenges and strategies for control, conversion and utilization of CO_2 for sustainable development involving energy, catalysis, adsorption and chemical processing. *Catal. Today* **2006**, *115*, 2–32. [CrossRef]

19. Janáky, C.; Hursán, D.; Endrődi, B.; Chanmanee, W.; Roy, D.; Liu, D.; de Tacconi, N.R.; Dennis, B.H.; Rajeshwar, K. Electro- and photoreduction of carbon dioxide: The twain shall meet at copper oxide/copper interfaces. *ACS Energy Lett.* **2016**, *1*, 332–338.

20. Leonard, D.P.; Pan, H.; Heagy, M.D. Photocatalyzed reduction of bicarbonate to formate: Effect of ZnS crystal structure and positive hole scavenger. *ACS Appl. Mater. Interfaces* **2015**, *7*, 24543–24549. [CrossRef]

21. Feaster, J.T.; Shi, G.; Cave, E.R.; Hatsukade, T.; Abram, D.N.; Kuhl, K.P.; Hahn, C.; Norskov, J.S.; Jaramillo, T.F. Understanding selectivity for the electrochemical reduction of carbon dioxide to formic acid and carbon monoxide on metal electrodes. *ACS Catal.* **2017**, *7*, 4822–4827. [CrossRef]

22. Pang, R.; Teramura, K.; Asakura, H.; Hosokawa, S.; Tanaka, T. Role of bicarbonate ions in aqueous solution as a carbon source for photocatalytic conversion of CO_2 into CO. *ACS Appl. Energy Mater.* **2019**, *2*, 5397–5405. [CrossRef]

23. NOAA National Centers for Environmental Information. *State of the Climate: Global Climate Report for June 2019*; NCEI: Asheville, NC, USA, 2019.

24. Harry-O'Kuru, R.E.; Biresaw, G.; Tisserat, B.; Evangelista, R. Synthesis of polyformate esters of vegetable oils: Milkweed, pennycress, and soy. *J. Lipids* **2016**, *2016*, 1–12. [CrossRef]

25. Jouny, M.; Luc, W.; Jiao, F. General techno-economic analysis of CO_2 electrolysis systems. *Ind. Eng. Chem. Res.* **2018**, *57*, 2165–2177. [CrossRef]

26. Afshar, A.A.N. *Chemical Profile: Formic Acid*; TranTech Consultants, Inc.: Philadelphia, PA, USA, 2014.

27. Bushuyev, O.; De Luna, P.; Dinh, C.T.; Tao, L.; Saur, G.; van de Lagemaat, J.; Kelley, S.O.; Sargent, E.H. What Should We Make with CO_2 and How Can We Make It? *Joule* **2018**, *2*, 825–832. [CrossRef]

28. Intergovernmental Panel on Climate Change. *Climate Change 2014: Synthesis Report*; IPCC: Geneva, Switzerland, 2014.

29. British Petroleum (BP). *Natural Gas*, 67th ed.; BP plc: London, UK, 2018.

30. Agarwal, A.S.; Zhai, Y.; Hill, D.; Sridhar, N. The electrochemical reduction of carbon dioxide to formate/formic acid: Engineering and economic feasibility. *ChemSusChem* **2011**, *4*, 1301–1310. [CrossRef] [PubMed]

31. Spurgeon, J.M.; Kumar, B. A comparative technoeconomic analysis of pathways for commercial electrochemical CO_2 reduction to liquid products. *Energy Environ. Sci.* **2018**, *11*, 1536–1551. [CrossRef]

32. Rumayor, M.; Dominguez-Ramos, A.; Perez, P.; Irabien, A. A techno-economic evaluation approach to the electrochemical reduction of CO_2 for formic acid manufacture. *J. CO_2 Util.* **2019**, *34*, 490–499. [CrossRef]

33. Halmann, M. Photoelectrochemical reduction of aqueous carbon dioxide on p-type gallium phosphide in liquid junction solar cells. *Nature* **1978**, *275*, 115. [CrossRef]

34. Inoue, T.; Fujishima, A.; Konishi, S.; Honda, K. Photoelectrocatalytic reduction of carbon dioxide in aqueous suspensions of semiconductor powders. *Nature* **1979**, *277*, 637. [CrossRef]

35. Ulman, M.; Aurian-Blajeni, B.; Halmann, M. Photoassisted carbon dioxide reduction to organic compounds using rare earth doped barium titanate and lithium niobate as photoactive agents. *Isr. J. Chem.* **1982**, *22*, 177–179. [CrossRef]

36. Aurian-Blajeni, B.; Halmann, M.; Manassen, J. Electrochemical measurement on the photoelectrochemical reduction of aqueous carbon dioxide on p-Gallium phosphide and p-Gallium arsenide semiconductor electrodes. *Sol. Energy Mater.* **1983**, *8*, 425–440. [CrossRef]

37. Halmann, M.; Katzir, V.; Borgarello, E.; Kiwi, J. Photoassisted carbon dioxide reduction on aqueous suspensions of titanium dioxide. *Sol. Energy Mater.* **1984**, *10*, 85–91. [CrossRef]

38. Inoue, H.; Moriwaki, H.; Maeda, K.; Yoneyama, H. Photoreduction of carbon dioxide using chalcogenide semiconductor microcrystals. *J. Photochem. Photobiol. A Chem.* **1995**, *86*, 191–196. [CrossRef]

39. Kanemoto, M.; Shiragami, T.; Pac, C.; Yanagida, S. Semiconductor photocatalysis. 13. Effective photoreduction of carbon dioxide catalyzed by zinc sulfide quantum crystallites with low density of surface defects. *J. Phys. Chem.* **1992**, *96*, 3521–3526. [CrossRef]

40. Johne, P.; Kisch, H. Photoreduction of carbon dioxide catalysed by free and supported zinc and cadmium sulphide powders. *J. Photochem. Photobiol. A Chem.* **1997**, *111*, 223–228. [CrossRef]

41. Pan, H.; Chowdhury, S.; Premachandra, D.; Olguin, S.; Heagy, M.D. Semiconductor photocatalysis of bicarbonate to solar fuels: Formate production from copper(I) oxide. *Acs. Sustain. Chem. Eng.* **2018**, *6*, 1872–1880. [CrossRef]

42. Pan, H.; Steiniger, A.; Heagy, M.D.; Chowdhury, S. Efficient production of formic acid by simultaneous photoreduction of bicarbonate and oxidation of glycerol on gold-TiO_2 composite under solar light. *J. CO_2 Util.* **2017**, *22*, 117–123. [CrossRef]

43. Pan, H.; Heagy, M.D. Plasmon-enhanced photocatalysis: Ag/TiO_2 nanocomposite for the photochemical reduction of bicarbonate to formic acid. *Mrs. Adv.* **2019**, *4*, 425–433. [CrossRef]

44. Beierle, A.; Gieri, P.; Pan, H.; Heagy, M.D.; Manjavacas, A.; Chowdhury, S. Titanium nitride nanoparticles for the efficient photocatalysis of bicarbonate into formate. *Sol. Energy Mater. Sol. Cells* **2019**, *200*, 109967. [CrossRef]

45. Baran, T.; Wojtyła, S.; Dibenedetto, A.; Aresta, M.; Macyk, W. Zinc sulfide functionalized with ruthenium nanoparticles for photocatalytic reduction of CO_2. *Appl. Catal. B Environ.* **2015**, *178*, 170–176. [CrossRef]

46. Kuwabata, S.; Nishida, K.; Tsuda, R.; Inoue, H.; Yoneyama, H. Photochemical reduction of carbon dioxide to methanol using ZnS microcrystallite as a photocatalyst in the presence of methanol dehydrogenase. *J. Electrochem. Soc.* **1994**, *141*, 1498–1503. [CrossRef]

47. Irvine, J.T.S.; Eggins, B.R.; Grimshaw, J. Solar energy fixation of carbon dioxide via cadmium sulphide and other semiconductor photocatalysts. *Sol. Energy* **1990**, *45*, 27–33. [CrossRef]

48. Eggins, B.R.; Robertson, P.K.J.; Murphy, E.P.; Woods, E.; Irvine, J.T.S. Factors affecting the photoelectrochemical fixation of carbon dioxide with semiconductor colloids. *J. Photochem. Photobiol. A Chem.* **1998**, *118*, 31–40. [CrossRef]

49. Henglein, A.; Gutiérrez, M.; Fischer, C.H. Photochemistry of colloidal metal sulfides 6. Kinetics of interfacial reactions at ZnS-Particles. *Ber. Der Bunsenges. Für Phys. Chem.* **1984**, *88*, 170–175. [CrossRef]

50. Kaneco, S.; Kurimoto, H.; Ohta, K.; Mizuno, T.; Saji, A. Photocatalytic reduction of CO_2 using TiO_2 powders in liquid CO_2 medium. *J. Photochem. Photobiol. A Chem.* **1997**, *109*, 59–63. [CrossRef]

51. Kaneco, S.; Shimizu, Y.; Ohta, K.; Mizuno, T. Photocatalytic reduction of high pressure carbon dioxide using TiO_2 powders with a positive hole scavenger. *J. Photochem. Photobiol. A Chem.* **1998**, *115*, 223–226. [CrossRef]

52. Kaneco, S.; Kurimoto, H.; Shimizu, Y.; Ohta, K.; Mizuno, T. Photocatalytic reduction of CO_2 using TiO_2 powders in supercritical fluid CO_2. *Energy* **1999**, *24*, 21–30. [CrossRef]

53. Liu, B.-J.; Torimoto, T.; Yoneyama, H. Photocatalytic reduction of CO_2 using surface-modified CdS photocatalysts in organic solvents. *J. Photochem. Photobiol. A Chem.* **1998**, *113*, 93–97. [CrossRef]

54. Kisch, H.; Lutz, P. Photoreduction of bicarbonate catalyzed by supported cadmium sulfide. *Photochem. Photobiol. Sci.* **2002**, *1*, 240–245. [CrossRef]

55. Zhang, X.V.; Martin, S.T.; Friend, C.M.; Schoonen, M.A.A.; Holland, H.D. Mineral-assisted pathways in prebiotic synthesis: Photoelectrochemical reduction of carbon(+IV) by manganese sulfide. *J. Am. Chem. Soc.* **2004**, *126*, 11247–11253. [CrossRef]

56. Xia, X.-H.; Jia, Z.-J.; Yu, Y.; Liang, Y.; Wang, Z.; Ma, L.-L. Preparation of multi-walled carbon nanotube supported TiO_2 and its photocatalytic activity in the reduction of CO_2 with H_2O. *Carbon* **2007**, *45*, 717–721. [CrossRef]

57. Qin, G.; Zhang, Y.; Ke, X.; Tong, X.; Sun, Z.; Liang, M.; Xue, S. Photocatalytic reduction of carbon dioxide to formic acid, formaldehyde, and methanol using dye-sensitized TiO_2 film. *Appl. Catal. B Environ.* **2013**, *129*, 599–605. [CrossRef]

58. Ulagappan, N.; Frei, H. Mechanistic study of CO_2 photoreduction in Ti silicalite molecular sieve by FT-IR spectroscopy. *J. Phys. Chem. A* **2000**, *104*, 7834–7839. [CrossRef]

59. Sato, S.; Morikawa, T.; Saeki, S.; Kajino, T.; Motohiro, T. Visible-light-induced selective CO_2 reduction utilizing a ruthenium complex electrocatalyst linked to a p-type nitrogen-doped Ta_2O_5 semiconductor. *Angew. Chem. Int. Ed.* **2010**, *49*, 5101–5105. [CrossRef] [PubMed]

60. Sato, S.; Arai, T.; Morikawa, T.; Uemura, K.; Suzuki, T.M.; Tanaka, H.; Kajino, T. Selective co_2 conversion to formate conjugated with H_2O oxidation utilizing semiconductor/complex hybrid photocatalysts. *J. Am. Chem. Soc.* **2011**, *133*, 15240–15243. [CrossRef] [PubMed]

61. Arai, T.; Tajima, S.; Sato, S.; Uemura, K.; Morikawa, T.; Kajino, T. Selective CO_2 conversion to formate in water using a CZTS photocathode modified with a ruthenium complex polymer. *Chem. Commun.* **2011**, *47*, 12664–12666. [CrossRef]

62. Suzuki, T.M.; Tanaka, H.; Morikawa, T.; Iwaki, M.; Sato, S.; Saeki, S.; Inoue, M.; Kajino, T.; Motohiro, T. Direct assembly synthesis of metal complex-semiconductor hybrid photocatalysts anchored by phosphonate for highly efficient CO_2 reduction. *Chem. Commun.* **2011**, *47*, 8673–8675. [CrossRef]

63. Iizuka, K.; Wato, T.; Miseki, Y.; Saito, K.; Kudo, A. Photocatalytic reduction of carbon dioxide over Ag cocatalyst-loaded $ALa_4Ti_4O_{15}$ (A = Ca, Sr, and Ba) using water as a reducing reagent. *J. Am. Chem. Soc.* **2011**, *133*, 20863–20868. [CrossRef]

64. Raja, K.S.; Smith, Y.R.; Kondamudi, N.; Manivannan, A.; Misra, M.; Subramanian, V. CO_2 photoreduction in the liquid phase over Pd-supported on TiO_2 nanotube and bismuth titanate photocatalysts. *Electrochem. Solid State Lett.* **2011**, *14*, F5–F8. [CrossRef]

65. Mendoza, J.A.; Kim, H.K.; Park, H.K.; Park, K.Y. Photocatalytic reduction of carbon dioxide using Co_3O_4 nanoparticles under visible light irradiation. *Korean J. Chem. Eng.* **2012**, *29*, 1483–1486. [CrossRef]

66. Qin, Z.; Tian, H.; Su, T.; Ji, H.; Guo, Z. Soft template inducted hydrothermal $BiYO_3$ catalysts for enhanced formic acid formation from the photocatalytic reduction of carbon dioxide. *Rsc Adv.* **2016**, *6*, 52665–52673. [CrossRef]

67. Ali, S.; Lee, J.; Kim, H.; Hwang, Y.; Razzaq, A.; Jung, J.-W.; Cho, C.-H.; In, S.-I. Sustained, photocatalytic CO_2 reduction to CH_4 in a continuous flow reactor by earth-abundant materials: Reduced titania-Cu_2O Z-scheme heterostructures. *Appl. Catal. B Environ.* **2020**, *279*, 119344. [CrossRef]

68. Yin, G.; Nishikawa, M.; Nosaka, Y.; Srinivasan, N.; Atarashi, D.; Sakai, E.; Miyauchi, M. photocatalytic carbon dioxide reduction by copper oxide nanocluster-grafted niobate nanosheets. *ACS Nano* **2015**, *9*, 2111–2119. [CrossRef] [PubMed]

69. Lan, Y.; Xie, Y.; Chen, J.; Hu, Z.; Cui, D. Selective photocatalytic CO_2 reduction on copper–titanium dioxide: A study of the relationship between CO production and H_2 suppression. *Chem. Commun.* **2019**, *55*, 8068–8071. [CrossRef] [PubMed]

70. Bae, K.-L.; Kim, J.; Lim, C.K.; Nam, K.M.; Song, H. Colloidal zinc oxide-copper(I) oxide nanocatalysts for selective aqueous photocatalytic carbon dioxide conversion into methane. *Nat. Commun.* **2017**, *8*, 1156. [CrossRef] [PubMed]

71. Nogueira, A.E.; Oliveira, J.A.; da Silva, G.T.S.T.; Ribeiro, C. Insights into the role of CuO in the CO_2 photoreduction process. *Sci. Rep.* **2019**, *9*, 1316. [CrossRef]

72. Dedong, Z.; Maimaiti, H.; Awati, A.; Yisilamu, G.; Fengchang, S.; Ming, W. Synthesis and photocatalytic CO_2 reduction performance of Cu_2O/Coal-based carbon nanoparticle composites. *Chem. Phys. Lett.* **2018**, *700*, 27–35. [CrossRef]

73. Zhang, F.; Li, Y.-H.; Qi, M.-Y.; Tang, Z.-R.; Xu, Y.-J. Boosting the activity and stability of Ag-Cu_2O/ZnO nanorods for photocatalytic CO_2 reduction. *Appl. Catal. B Environ.* **2020**, *268*, 118380. [CrossRef]

74. Aguirre, M.E.; Zhou, R.; Eugene, A.J.; Guzman, M.I.; Grela, M.A. Cu_2O/TiO_2 heterostructures for CO_2 reduction through a direct Z-scheme: Protecting Cu_2O from photocorrosion. *Appl. Catal. B Environ.* **2017**, *217*, 485–493. [CrossRef]

75. Park, S.-M.; Razzaq, A.; Park, Y.H.; Sorcar, S.; Park, Y.; Grimes, C.A.; In, S.-I. Hybrid Cu_xO–TiO_2 Heterostructured Composites for Photocatalytic CO_2 Reduction into Methane Using Solar Irradiation: Sunlight into Fuel. *ACS Omega* **2016**, *1*, 868–875. [CrossRef]

76. Gusain, R.; Kumar, P.; Sharma, O.P.; Jain, S.L.; Khatri, O.P. Reduced graphene oxide–CuO nanocomposites for photocatalytic conversion of CO_2 into methanol under visible light irradiation. *Appl. Catal. B Environ.* **2016**, *181*, 352–362. [CrossRef]

77. Zhai, Q.; Xie, S.; Fan, W.; Zhang, Q.; Wang, Y.; Deng, W.; Wang, Y. Photocatalytic Conversion of carbon dioxide with water into methane: Platinum and copper(I) oxide Co-catalysts with a core–shell structure. *Angew. Chem. Int. Ed.* **2013**, *52*, 5776–5779. [CrossRef]

78. Wu, Y.A.; McNulty, I.; Liu, C.; Lau, K.C.; Liu, Q.; Paulikas, A.P.; Sun, C.-J.; Cai, Z.; Guest, J.R.; Ren, Y.; et al. Facet-dependent active sites of a single Cu_2O particle photocatalyst for CO_2 reduction to methanol. *Nat. Energy* **2019**, *4*, 957–968. [CrossRef]

79. Mele, G.; Annese, C.; De Riccardis, A.; Fusco, C.; Palmisano, L.; Vasapollo, G.; D'Accolti, L. Turning lipophilic phthalocyanines/TiO_2 composites into efficient photocatalysts for the conversion of CO_2 into formic acid under UV–vis light irradiation. *Appl. Catal. A Gen.* **2014**, *481*, 169–172. [CrossRef]

80. Premkumar, J.; Ramaraj, R. Photocatalytic reduction of carbon dioxide to formic acid at porphyrin and phthalocyanine adsorbed Nafion membranes. *J. Photochem. Photobiol. A Chem.* **1997**, *110*, 53–58. [CrossRef]

81. Rajan Premkumar, J.; Ramaraj, R. Photoreduction of carbon dioxide by metal phthalocyanine adsorbed Nafion membrane. *Chem. Commun.* **1997**, *4*, 343–344. [CrossRef]

82. Liu, S.; Zhao, Z.; Wang, Z. Photocatalytic reduction of carbon dioxide using sol-gel derived titania-supported CoPc catalysts. *Photochem. Photobiol. Sci.* **2007**, *6*, 695–700. [CrossRef]

83. Zhao, Z.; Fan, J.; Xie, M.; Wang, Z. Photo-catalytic reduction of carbon dioxide with in-situ synthesized CoPc/TiO_2 under visible light irradiation. *J. Clean. Prod.* **2009**, *17*, 1025–1029. [CrossRef]

84. Yazdanpour, N.; Sharifnia, S. Photocatalytic conversion of greenhouse gases (CO_2 and CH_4) using copper phthalocyanine modified TiO_2. *Sol. Energy Mater. Sol. Cells* **2013**, *118*, 1–8. [CrossRef]

85. Mele, G.; Annese, C.; Accolti, L.; De Riccardis, A.; Fusco, C.; Palmisano, L.; Scarlino, A.; Vasapollo, G. Photoreduction of carbon dioxide to formic acid in aqueous suspension: A comparison between phthalocyanine/TiO_2 and porphyrin/TiO_2 catalysed processes. *Molecules* **2015**, *20*, 396–415. [CrossRef]

86. Conner, W.C.; Falconer, J.L. Spillover in Heterogeneous Catalysis. *Chem. Rev.* **1995**, *95*, 759–788. [CrossRef]

87. Gangu, K.K.; Maddila, S.; Mukkamala, S.B.; Jonnalagadda, S.B. A review on contemporary metal–organic framework materials. *Inorg. Chim. Acta* **2016**, *446*, 61–74. [CrossRef]

88. Sun, D.; Fu, Y.; Liu, W.; Ye, L.; Wang, D.; Yang, L.; Fu, X.; Li, Z. Studies on photocatalytic CO_2 reduction over NH_2-Uio-66(Zr) and its derivatives: Towards a better understanding of photocatalysis on metal–organic frameworks. *Chem. A Eur. J.* **2013**, *19*, 14279–14285. [CrossRef] [PubMed]

89. Wang, D.; Huang, R.; Liu, W.; Sun, D.; Li, Z. Fe-based MOFs for photocatalytic CO_2 reduction: Role of coordination unsaturated sites and dual excitation pathways. *Acs Catal.* **2014**, *4*, 4254–4260. [CrossRef]

90. Fu, Y.; Sun, D.; Chen, Y.; Huang, R.; Ding, Z.; Fu, X.; Li, Z. An amine-functionalized titanium metal–organic framework photocatalyst with visible-light-induced activity for CO_2 reduction. *Angew. Chem. Int. Ed.* **2012**, *51*, 3364–3367. [CrossRef] [PubMed]

91. Fei, H.; Sampson, M.D.; Lee, Y.; Kubiak, C.P.; Cohen, S.M. Photocatalytic CO_2 reduction to formate using a Mn(I) molecular catalyst in a robust metal–organic framework. *Inorg. Chem.* **2015**, *54*, 6821–6828. [CrossRef] [PubMed]

92. Lee, Y.; Kim, S.; Kang, J.K.; Cohen, S.M. Photocatalytic CO_2 reduction by a mixed metal (Zr/Ti), mixed ligand metal-organic framework under visible light irradiation. *Chem. Commun.* **2015**, *51*, 5735–5738. [CrossRef] [PubMed]